AD689444

TR-1428

FLUERICS
27. FLUERIC TEMPERATURE-SENSING
OSCILLATOR DESIGN

April 1969

DDC

JUL 8 1969

A

U.S. ARMY MATERIEL COMMAND

HARRY DIAMOND LABORATORIES

WASHINGTON, D.C. 20438

AD

TR-1428

FLUERICS
27. FLUERIC TEMPERATURE-SENSING OSCILLATOR DESIGN

by

Wilmer Gaylord
Vondell Carter

April 1969

U.S. ARMY MATERIEL COMMAND

HARRY DIAMOND LABORATORIES

WASHINGTON, D.C. 20438

1

BLANK PAGE

A B S T R A C T

Studies have been conducted at the Harry Diamond Laboratories to determine the dependence of output-signal characteristics on cavity (resonator) dimensions of flueric temperature-sensing oscillators. The effects of resonator dimensions (length and width), of nozzle area ratio, and of edge distance from the inlet nozzle on the operational threshold, frequency, amplitude, and signal-isolation ratio were studied.

The information derived can be utilized to make the process of flueric temperature sensor-oscillator design a more precise and scientific operation. Experimental data have been arranged to show the relationship of signal characteristics to resonator configuration (dimensions) and environment (pressure and temperature).

P R E F A C E

This report is a direct result of research conducted on flueric temperature sensors at the Harry Diamond Laboratories since 1962. The effort between 1962 and 1964 was sponsored by the Air Force Propulsion Laboratory of the Aeronautical Systems Division at Wright-Patterson Air Force Base (WPAFB), Ohio. More recently (Sept 1965 to Sept 1966), an advanced research effort was supported partially by the U. S. Army Aviation Laboratories (AAL), Fort Eustis, Virginia.

The original guidance and review of objectives by Charles Bentz and other Air Force personnel, as well as the more recent advice of L. E. Bell and others at AAL are greatly appreciated. The authors also wish to acknowledge contributions by Richard Gottron, who was one of the pioneers in flueric temperature sensing at HDL. Also, the authors appreciated the assistance of HDL staff members Eugene Flester in designing various test devices and Leland Ray Jones in conducting most of the tests, as well as his contributions in data collection, evaluation, and arrangement.

The illustrative material on pages 64 through 67 was extracted from Air Tables developed by D. P. Jordan and M. D. Mintz (copyright, 1965), and is included with permission of McGraw Hill Book Company.

4

CONTENTS

6

1. INTRODUCTION

A research program has been conducted at these laboratories to determine the dependence of output-signal characteristics on cavity (resonator) dimensions of flueric temperature-sensing oscillators. This report represents an effort to combine and arrange the research data accumulated on the design and operation of these sensors.

The flueric temperature sensor is a temperature-sensitive oscillator. Its temperature sensitivity is based on the fact that the velocity of propagation of a pressure pulse in a gas is dependent upon the absolute temperature of that gas. The simplest type fluid oscillator, or at least the easiest to visualize, is illustrated in figure 1. This oscillator is essentially a bistable fluid amplifier with feedback loops. Initially, the jet attaches to and flows down one leg. As a result of the flow down this leg, a pressure pulse propagates around the feedback loop at acoustic velocity and switches the jet to the opposite leg. The process is repeated on the side, thus completing a cycle. The period for such an oscillator is approximately

$$\text{Period} = \frac{2L}{a} + S_t \tag{1}$$

where

S_t = the switching time,

L = the length of one loop, and

a = the speed of sound in the gas.

If S_t is very small, then the frequency is approximately

$$f = \frac{a}{2L} = \frac{(\gamma RT)^{1/2}}{2L} \tag{2}$$

where γ is the ratio of specific heats, R is the gas constant, and T is the temperature ($^\circ$K).

The oscillators that have been used most frequently as temperature sensors are the jet-edge and resonator type. Jet-edge oscillation occurs when a solid body (wedge) is placed in a stream that is issuing from a nozzle as shown in figure 2. An empirical equation for the jet-edge or edgetone frequency, f_e, was derived by G. Brown [1]*

$$f_e = 0.466 \, j(u-40)(1/h-0.07), \tag{3}$$

where j is an experimentally determined constant equal to 1, 2.3, 3.8, or 5.4 (corresponding to the stage of jet oscillation),

u is the jet velocity in cm/sec, and

h is the distance from the jet outlet to the edge in centimeters.

The constants 40 and 0.07 were experimentally determined. These constants may be neglected without introducing appreciable error, since u >> 40 and 1/h >> 0.07. Also, for the usual sensor designs, j is equal to 1; then

---

*Numbers in brackets indicate literature references at the end of this report.

$$f_e = 0.466 \ u/h. \tag{3a}$$

If the jet-edge system is inclosed by a resonator system (cavities) as shown in figure 3, a coupling of the jet-edge and cavity eigenfrequencies will occur. A resonating cavity tunes the jet-edge frequency at approximately the cavity eigenfrequencies, f_n, expressed by

$$f_n = \frac{(n-1/2)a}{2(L_o + e)} \ , \tag{4}$$

where

n is an integer 1, 2, 3...(n = 1 yields the fundamental frequency),

a is the speed of sound (cm/sec),

L_o is the cavity length (cm) in the direction of pulse propagation, and

e is a small correction which is usually neglected.

In all except special cases in sensor design n is unity; and if e is neglected, equation (4) becomes

$$f_1 = \frac{a}{4L_o} \ . \tag{4a}$$

Since

$$a = (\gamma RT)^{1/2}$$

$$f_1 = \frac{(\gamma RT)^{1/2}}{4L_o} \ , \tag{4b}$$

As shown in figure 4, coupling occurs near the intersection of the f_e and f_n lines. The frequency increases with increasing velocity. If the velocity reaches a value corresponding to the value at the intersection of the second cavity eigenfrequency line (n = 2) and the f_e line, the frequency will jump to the third harmonic, as can be seen in equation (4) when n=2. If, however, the total exhaust area, A_e, is sufficiently less than the total inlet area in the jet-edge and resonator system shown in figure 3, the jump will not occur. The smaller outlet area will limit the velocity at the outlet; thus, the second intersection is not reached.

The following sections describe the experimental studies conducted and the design and operating details of the flueric temperature sensor.

2.   EXPERIMENTAL INVESTIGATION

A major portion of the experimental information presented in this report was generated with the model shown in figure 5. The remaining information was obtained with experimental models and sensors designed for specific purposes and constructed during the early phases of the state-of-the-art.

2.1   Experimental Model

The experimental model in figure 5 was constructed to allow independent adjustment of L, h, and b. Dimension L_θ was varied by removing or adding the spacers shown. The output signal was monitored at the point shown for all tests. The dimensions of this model were somewhat larger than those for the usual sensor. The size was a feature of the design that made the experiment a less tedious endeavor than would have been the case for a smaller device. There appears to be no difficulty in applying the information obtained with this model to sensors with much smaller dimensions.

2.2   Apparatus

The apparatus used in conducting these investigations can be described generally by the schematic diagram in figure 6. The equipment depicted here permitted the following quantities to be measured, recorded, or monitored as the objective required:

(1)   Input pressure to the sensor, p_i;

(2)   Sensor cavity pressure--both steady-state and oscillatory (p_c and p_{out}) where the oscillatory component is the sensor output signal, p_{out};

(3)   Frequency of the output signal, f;

(4)   Waveform of output signal; and

(5)   Harmonic content of the output signal.

The air supply used is in general the common shop variety and is rated at approximately 600 kN/m^2 (gage) maximum pressure. Some experiments have been conducted, however, with input pressures as high as 1200 kN/m^2 (g). The input pressure p_i to the sensor is measured immediately upstream of the input nozzle, and the sensor exhausts to atmospheric conditions unless some other specific environment is established.

The output signal of the sensor is detected by a dynamic pressure transducer located on a transmission line extending from the sensor cavity. It is the usual practice to simulate an infinite transmission line by attaching a section of transmission tubing of approximately 1.5 m in length. The tubing is then deadended with a static pressure gage, for measuring the cavity pressure p_c.

The signal from the transducer is processed through an amplifier, displayed on an oscilloscope, and then fed to a wave analyzer where the harmonic content can be measured. Parallel with the oscilloscope and wave analyzer are an amplifier, an active electronic filter, and a counter (digital frequency meter). The filter shown in the dotted outline of figure 6 may be required when testing at high temperatures where the signal amplitude may be relatively small.

For experimental studies where elevated temperatures are required, or for sensor calibration, the apparatus shown in figure 7 is used. The air supply and electronic instrumentation used are the same as those previously described. The source of heat is an electrical-resistance-heated oven into which the sensor is placed. The air supplied to the sensor is heated by passing it through a coil of tubing (6 to 8 m in length), which is also mounted in the oven immediately upstream of the sensor.

9

A thermocouple, mounted at the entrance of the input nozzle, measures the temperature of the incoming gas. Readout of the temperature is accomplished with a standard millivolt potenticmeter.

Although the signal-detection system is essentially the same as in figure 6, precautions must be taken to protect the dynamic pressure transducer from high-temperature damage and to preserve its calibration factor. In our experiments, a rather simple water-jacket-type cooling fixture was mounted on the transmission line adjacent to the exterior wall of the oven and separating the transducer from the hot zone. The temperature of the transducer was thus maintained within safe limits.

2.3   Results

The results of these experimental investigations are presented in section 3 of this report, together with certain theoretical considerations. An attempt has been made to present the material as a design guide to the individual who wishes to build a flueric temperature sensor that will have reasonably predictable performance characteristics. Toward this end, the data have in some instances been nondimensionalized. On the other hand, to maintain a feel for the phenomena being described, the absolute magnitudes of the measured variables and geometric parameters are included.

3.   DESCRIPTION OF SENSOR DESIGN

The attractive features of the flueric temperature sensor include its ability to perform in very high-temperature environments. The sensor is limited in high-temperature measurement capability, primarily by the material from which it is fabricated.

3.1   Design Considerations — Performance

In general, the primary considerations in design are determined by the service environmental conditions. These include type of gas, temperature, pressure, and velocity. The sensor, then, must be designed around these factors, if the desired performance characteristics are to be realized.

The signal characteristics that usually receive most attention in design are:

(1)   Operational threshold,

(2)   Output frequency,

(3)   Sensitivity,

(4)   Signal amplitude,

(5)   Pressure (or velocity) dependence, and

(6)   Time response.

The sensor configuration affects all the above characteristics. In equations (3) and (4), h and L_0 are the sensor dimensions that affect

10

performance characteristics. These and other dimensions that affect performance are shown in figure 5. Most significant of the dimensions shown are h, L_0, and b. The specific influence of each dimension will be covered in the discussion of the individual performance characteristics.

3.1.1 Operational Threshold

The threshold pressure or velocity is the point where coupled oscillation begins and is maintained. It can be explained with the aid of figures 8 and 9. Figure 8 shows theoretical frequencies f_e and f_1 as a function of velocity. The edgetone frequency, f_e or f_e', begins at low velocity and has a constant slope that is inversely proportional to h. The edgetone frequency couples with or tunes the cavity eigenfrequency near the intersection of the f_e and f_1 lines. The theoretical intersection of these lines (eq 3a and 4a) indicates the approximate velocity at the threshold. The lower threshold for f_e' is true because $h' < h_1$. In figure 9, the cavity eigenfrequency f_1 and jet-edge frequency f_e are shown as a function of power jet pressure. The intersection of the f_e and f_1 lines indicates the approximate value of the inlet pressure at the threshold p_{i_t}. The extent of variation of the

actual threshold from the intersection as shown in figures 8 and 9 is a function of the ratio of the inlet nozzle area to the exhaust nozzle area, the splitter distance, and the breadth of the cavity. The nozzle area ratio determines the pressure-velocity relationship, and thus affects mass flow at the threshold.

The point of intersection of f_e and f_1 is a function of the ratio h/L_0. Figure 10 shows that the threshold u_i may be identical for different values of L and h if h/L_0 is constant.

Figure 11 shows that a considerable variation in threshold can occur for a variation in cavity breadth. Threshold pressure decreases as breadth increases, and has greater dependence on breadth for larger values of h (fig. 11). Figure 12 shows the threshold pressure plotted against the h/L_0 ratio for three values of b.

Figures 8 through 12 show that the threshold is a function of the ratio h/L_0, nozzle area ratio, and cavity breadth. The significant trends are: (1) For $h/L_0 = 0.20$ or less, very small changes in threshold pressure occur for variations of b; whereas for $h/L_0 = 0.33$ or greater, the threshold pressure varies by as much as a factor of five or more for the same variation of b. (2) All the curves indicate that as h/L_0 increases, the threshold increases, corresponding to a decrease in the slope of the f_e line.

3.1.2 Output Frequency

The output signal of a jet-edge resonator-type oscillator is essentially a sine wave. Some typical output signals are shown in figure 13. The signal is initiated at the threshold pressure and is continuous as a function of input pressure. Except at pressures very near the threshold, frequency does not vary appreciably as a function of inlet pressure.

11

The frequency of the signal over a given pressure range can be segmented as shown in figure 14. The significant designations are as follows:

(1) A designates the threshold frequency and B the corresponding pressure.

(2) C designates the frequency at choked flow,[1] and D the corresponding pressure.

(3) The frequency at any pressure above choked flow is designated by E and may increase slightly with increasing p_i. The output frequency at the designated points is related to h, L_0, b, and area ratio, A_e/A_i.

Effect of Area Ratio.—In general, the ratio of the exhaust nozzle area, A_e/A_i, is less than unity. Area ratios used in sensor design are generally in the range of 0.50 to 0.90. An area ratio that is less than 1 serves primarily to:

(1) Limit pressure dependence by fixing the choked flow point (C in fig. 14); and

(2) Limit the inlet velocity to a value less than the value at the intersection of the f_c and f_2 lines (fig. 4), so that the frequency does not jump to the second cavity eigenfrequency (third harmonic).

The effect of area ratio on the choked flow point is shown in figure 15. Choked flow occurs in the exhaust nozzle at higher inlet pressures for larger area ratios. Since the choked flow point occurs at lower input pressures for smaller areas ratios, a given sensor has a smaller region of pressure dependence D (fig. 14) for small area ratios than that for large area ratios.

Effect of h, L_0, and b.—The splitter distance h and cavity dimensions L_0 and b have a significant effect on the output frequency. The effect is present over the total pressure range.

The inverse relationship between output frequency and b is indicated by the curves in figure 16, which show frequency as a function of input pressure for five values of breadth. The higher frequencies for the smaller values of breadth indicate a significant dependence of output frequency on breadth. Figure 17 shows the relationship between breadth b and frequency for two constant values of h (two curves) and for corrected h. The corrected h, h_c, is the adjusted value of h at each value of b which yields maximum signal amplitude. Since amplitude varies significantly with h (as is shown in the next section), for design purposes it is desirable to know h_c for each value of b. The curve for h_c can be easily contrasted with the curves for constant h by the difference in general slope.

---

[1]The choked flow point corresponds to the input pressure p_i^*, beyond which velocity (consequently frequency) ceases to increase as pressure increases. For this condition $p_e/p_c \leq 0.53$ and $p_c/p_i \approx$ constant.

Output frequency is related to h as shown in figure 18. Curves are shown for seven values of b. The locus of values of h that yield maximum signal amplitude for each value of b is shown; the theoretical frequency derived in equation is also shown.

The data in figures 17 and 18 show that equation (4) is limited in accurately predicting output frequency. Only the points on the curve for b = 1.5 cm in figure 18 yield output frequencies that are within approximately 10 percent of the value predicted by equation (4). These data points indicate that equation (4) predicts the output frequency within 10 percent when b/L is less than 0.4. Equation (4) was modified to give a more accurate prediction of output frequency for a larger range of values of b and h. The empirically derived equation predicts output frequency as a function of L_0, b, and corrected h; the derivation was based on the assumption that the wave traverses a triangular path. The relationship is as follows:

$$f_{out} = \frac{a}{2\left[\sqrt{L_0^2 + (b - h/2)^2} + (b - h/2) + L_0\right]} \tag{5}$$

A comparison of experimental output frequencies and the frequencies predicted by equation (5) is shown in figure 19. The agreement is within 3 percent for small values of b and 1.8 percent for large values of b. This agreement indicates that the accuracy of prediction obtainable is more than adequate for all forseeable requirements.

3.1.3 Signal Amplitude

The amplitude of the output signal of a flueric temperature sensor is defined as the peak-to-peak value of the oscillatory cavity pressure, as illustrated in figure 20. The output pressure may be measured by a transducer located either at the cavity or at some station on a transmission line from the cavity. The flueric signal may also be transmitted to some other flueric device where it is operated upon as desired. It is the requirement for transmission that establishes a design criterion for sensor output signal amplitude; that is, the signal must be of sufficient strength at the point of generation (the cavity) to tolerate the attenuation associated with transmission to the point where the signal is to be utilized.

Amplitude as a Function of Input Conditions — For a sensor with some fixed geometry, a typical experimentally obtained plot of output pressure P_{out} versus input pressure p_i is illustrated in figure 21. The curve is nonlinear for small values of p_i, with dP_{out}/dp_i decreasing as p_i increases. As $p_i = p_i^*$ is approached, the curve becomes linear and remains so for all larger values of p_i.

The plot in figure 21 suggests that P_{out} is proportional to the mass flux, in which case

$$P_{out} = K_1 \rho u \qquad (gm/cm^2 \ sec).$$

The standard relationships for a frictionless adiabatic process allow us to write

13

$$P_{out} = K_1 \rho u = K_2 \left[1 - \left(\frac{p_c}{p_i}\right)^{\frac{\gamma-1}{\gamma}} \right]^{1/2} \cdot \rho_i \left(\frac{p_c}{p_i}\right)^{\frac{1}{\gamma}}. \tag{6}$$

where

p_c = cavity steady-state pressure for a constant temperature input condition. If

$$\frac{p_c}{p_i} = \text{const, for } p_i > p_i^*,$$

$$P_{out} = K_2 \cdot K_3 \cdot \rho_i K_4;$$

where

$$\rho_i = \frac{p_i}{p_{std}} \rho_{std}$$

Thus, $\quad P_{out} = K_5 p_i \tag{7}$

for p_i greater than the value that produces choked flow at the sensor exhaust — that is, $> p_i^*$ (the usual region of operation).

If the input gas temperature is not constant, a more complete expression for the output signal amplitude is

$$P_{out} = K_1 u \rho = \sqrt{\left(\frac{2}{\gamma-1}\right) \frac{\gamma p_i}{\rho_i} \left[1 - \left\{\frac{p_c}{p_i}\right\}^{\frac{\gamma-1}{\gamma}} \right]} \cdot \rho_i \left(\frac{p_c}{p_i}\right)^{1/\gamma} \tag{8}$$

$$= K_6 \, a_i \left[1 - \left(\frac{p_c}{p_i}\right)^{\frac{\gamma-1}{\gamma}} \right]^{1/2} \cdot \rho_i \left(\frac{p_c}{p_i}\right)^{1/\gamma}$$

where a_i is the velocity of sound in the input reservoir.

But, $\quad \rho_i = \frac{p_i}{p_{std}} \cdot \frac{T_{std}}{T_i} \rho_{std}$

and $\quad a_i = (\gamma R T_i)^{1/2}$

thus, $P_{out} = K_7 \, T_i^{1/2} \left[1 - \left(\frac{p_c}{p_i}\right)^{\frac{\gamma-1}{\gamma}} \right]^{1/2} \cdot \frac{p_i}{T_i} \left(\frac{p_c}{p_i}\right)^{1/\gamma} . \tag{8a}$

Therefore given a value of $p_i > p_i^*$, the output signal amplitude is seen to be inversely proportional to the square root of the temperature:

$$P_{out} = K_8 T^{-1/2} \tag{9}$$

Figure 22 shows this characteristic for data obtained with a miniature sensor and plotted with theoretical curves based on equation (9). However, for a miniature sensor the speed of wave propagation would actually be

14

$$a_i = (\gamma R T)^\alpha,$$

where

$$\alpha < 1/2 ;$$

this variation is due to the viscous effects present in the very small devices (see section 3.1.5). Substitution in equation (8a) would change equation (9) to

$$P_{out} = K_8 T^{-\beta} \tag{9a}$$

where

$$\beta = (1-\alpha) \overset{\geq}{=} 1/2$$

Thus, P_{out} would decay somewhat more rapidly than indicated by the theoretical curves shown in figure 22.

Amplitude as a Function of Geometry. — The internal geometry of a flueric temperature sensor can significantly affect the signal amplitude. The dimensions that have been primarily considered here are cavity length L_0, cavity width (or breadth) b, and splitter distance h.

Accepted theory and experiments indicate that the resonance of a cavity is affected by the volume of the cavity and the area of the mouth. In the devices considered here where the thickness or depth is constant, the area of the mouth is directly proportional to h and (for a given L_0) the cavity volume is directly proportional to b. In addition to affecting the cavity configuration, h influences the frequency of the exciting force, the jet. Based on other resonating systems, it seems reasonable to expect that the largest signal amplitudes will be obtained when the frequency of the exciting force corresponds to the resonant frequency of the cavity. Thus, some significant dependence of amplitude on h is to be expected.

Figures 23 and 24 illustrate the effect of the relationship between h and b on the propagation of a pressure wave. When b is large and h is small, the wave front will be somewhat cylindrical. As b becomes smaller and h approaches b, the wave front becomes more planar. In the case of the cylindrical wave, considerably more dispersion of the wave occurs than in the planewave case. Consequently, configurations of the latter type (fig. 24) should yield appreciably higher amplitudes.

In figure 25, the signal amplitude is presented as a function of splitter distance for a given value of L_0 and with b as a parameter. Significant here are the facts that: (1) for each value of b there is a unique value for h, which yields a maximum pressure amplitude; and (2) the maximum amplitude decreases as b increases. The dashed curve in the plot (fig. 25) is the locus of the maximum amplitude points. The data are in good general agreement with previously mentioned considerations regarding cavity resonance.

These same data have been plotted as a function of b with h as a parameter in figure 26. Note that the maximum amplitude points for given values of h differ from the maximum amplitude points of

figure 25. For a particular sensor design, the set of curves to be used would be determined by the flexibility possible with one or the other of the dimensions (h or b). The dashed curves of figure 25 and 26 are based upon the consideration that b is the independent dimension with respect to h — that is, it is assumed that a required or desired value of b has been determined, and that a value of h which will yield a maximum output signal for that value of b is desired.

Since the cavity mouth must communicate the exciting force to a cavity of some given cross-sectional area (proportional to b), it seems reasonable to consider the ratio h/b. For a given value of L_0, cavity size and shape can be indicated by the ratio b/L_0. Plotting the output signal data as a function of these nondimensionalized quantities yields figure 27. Again, the maximum amplitude points can be uniquely located — in this case in terms of h/b and b/L_0. In addition, it appears that the locus of these points can now be described by a straight line passing through the origin — that is,

$$\frac{P_{out_{max}}}{P_i} = m_1 \ (\frac{h}{b}) , \tag{10}$$

where m_1 is a constant determined by L_0, m_2 by L_{0_2}, etc (changing inversely with L_0), and

$$\frac{h}{b} = G \ (\frac{b}{L_0} , \ L_0) \quad .$$

Figure 28 relates h/b to b/L for three values of L_0. Note that the dependence of h/b on b/L_0 becomes quite small as $b/L_0 \rightarrow 1.5$, but is significant for $b/L_0 < 0.5$. However, some values of these variables have little or no physical significance; for example, a value of $h/b > 1$ indicates a splitter distance greater than the cavity width, which is at present meaningless.

To relate h/b, b/L and P_{out}, a grid construction such as that shown in figure 29 is necessary. The ratio b/L_0 is the independent variable, P_{out} the dependent variable, and h/b and L_0 parameters. An interesting characteristic exists in the fact that for $L_0 < 2.46$ cm, h/b approaches a constant value for a given value of b/L_0.

For the three values of L_0 shown, the input and output nozzle dimensions were not altered; consequently, the mass flux through the sensor remained constant for a constant input pressure. It was therefore reasonable to expect that amplitude would increase with a decrease in L; for while the input energy remained the same, the volume and thus the energy requirement of the cavity was decreasing. This is in contrast to the case of sensor miniaturization, wherein the mass flux is scaled in approximately the same ratio as cavity dimensions. In this latter case, the dependence of amplitude upon L_0 does not exist.

3.1.4 Signal-Isolation Ratio and Signal Quality

The sensor output signal usually contains harmonic distortion generated in the sensor or in the transmission system. It is the level of this harmonic distortion that is indicated by the use of the signal-isolation ratio.

16

The signal-isolation ratio is defined as the ratio of the amplitude of the fundamental frequency to that of the second harmonic, that is,

$$Si = \frac{P'_{out}}{P''_{out}}$$

where P'_{out} is the amplitude of the fundamental, and P''_{out} is the amplitude of the second harmonic. Figures 30 and 31 show curves that are characteristic of the quantity as a function of input pressure and as a function of temperature, respectively.

In figure 30, it may be observed that Si decays quite rapidly as p_i increases for small values of p_i, generally below 100 kN/m^2 (g). For larger values of p_i, the ratio remains approximately constant; in some instances, a slight increase or decrease is observed. At the small values of p_i the fluid equations are nearly linear; there is not sufficient energy available at the input to produce a significant harmonic amplitude in addition to the fundamental; nearly all the energy that is converted to cavity resonance is dissipated in the fundamental. At the larger values of p_i, sufficient energy is available, and is apparently distributed among the fundamental and its harmonics in a nearly constant proportion. Thus, Si remains constant, while the amplitudes of the fundamental and the harmonics increase with p_i.

The relationship of signal-isolation ratio to input temperature for a given sensor is shown in figure 31. Several input pressures are plotted, which indicate that the values are smaller at the higher pressures. Significant here is the fact that Si increases with temperature. This is the result of the decrease in mass flux, and thus input energy, associated with the temperature increase for a constant input pressure. The situation is comparable to operating at a lower input pressure for a constant temperature.

Interestingly, figure 31 reveals that a larger variation of Si occurs with changes of input pressure at the high temperatures than that occurring at low temperatures. This can be explained by the plot of Si versus p_i, where it may be noted that the largest variations in Si prevail at the small values of p_i — that is, relatively low levels of input mass flux. Operating the sensor at elevated temperatures produces a similar low-level mass flux condition. Thus, changes of the input pressure under such a condition yield a behavior similar to that for small input pressures at room temperature (see fig. 30).

The effects of geometric parameters on signal-isolation ratio are shown in figures 32 and 33. Figure 32 indicates that as cavity width b increases, the signal-isolation ratio increases rapidly. This seems consistent with previous observations if we consider that the energy density in the wave decreases with an increase in b (for a constant L_0). The data points in figure 32 represent configurations for which h was adjusted to obtain maximum output amplitude for that particular value of b.

The behavior of signal-isolation ratio as a function of splitter distance is shown in figure 33. Each curve represents a constant value for b. As indicated by the Si versus b curve (fig. 32), the mean levels of the curves decrease with decreasing cavity width. At both extremes of the range of h, relatively large values of Si are obtained; this is true for all values of b investigated. These extreme

values of h represent configurations for which signal amplitude is relatively small.

The most significant characteristic of these curves, however, is that the center peak values for Si occur at or very near the maximum amplitude values for h (b = constant). If the maximum amplitude configuration is one for which the most efficient coupling occurs, then it would seem reasonable to consider that this most efficient process would be one in which the largest amount of energy would be dissipated in the fundamental resonant frequency. Thus Si should be large.

It becomes a somewhat arbitrary matter to decide what will be considered an acceptable isolation ratio. Presently, Si = 4 is considered satisfactory.

Besides the inherent nonlinearity of the fluid equations, a number of other factors have been identified as causes of distortion in the measured signal:

(1) Leaks— these may be internal to the sensor, at junctions of the transmission line, or at the adapter for a pressure transducer.

(2) Transmission line discontinuities.

(3) Transducer adapter internal geometry.

(4) Transducer mounting technique.

Little need be said concerning the elimination of leaks, and discontinuities in the transmission line; attention to fabrication procedures is, of course, the answer. However, transducer adapter design and mounting can become quite involved. Unfortunately, adequate guidance from manufacturers is not always available. The philosophy in the experimental work here has been to approach as closely as possible a mounting that is flush with the inner surface of the transmission line. Further discussion of signal transmission is contained in section 3.2.3.

3.1.5 Sensitivity

The theoretical output frequency for a flueric temperature sensor is given by equation (4b) as

$$f_n = \frac{(n - 1/2)\,(\gamma R T)^{1/2}}{2(L_0 + e)}$$

Thus, the sensitivity is defined to be

$$\frac{df_n}{dT} = \frac{(n - 1/2)(\gamma R)^{1/2}}{4(L_0 + e)} \cdot T^{-1/2}. \tag{11}$$

Written more simply, we have

$$\frac{df_n}{dT} = k T^{-1/2} \tag{11a}$$

18

from which we can observe that sensitivity will vary inversely with the square root of temperature.

The dependence of k on the cavity length L_0 is significant, for it indicates that miniaturization of the sensor (small values of L_0) yields high sensitivity. As shown in equation (5), the actual acoustic path length is dependent upon the cavity geometry including h, L_0, and b.

The factor k also depends upon several other quantities, two of which (γ and R) are relatively constant—except at extremely high temperatures and under conditions for which ionization of the gas occurs.* Although sensitivity can be increased by operating at the higher cavity eigenfrequencies (n =2,3,etc), it has proved practicable to design sensors for operation at the first eigenfrequency, or n = 1.

In relatively large sensors the speed of wave propagation in the sensor is essentially the speed of propagation in free air (i.e., in the atmosphere):

$$a = (\gamma RT)^{1/2}$$

However, for sensors of the small size most often used, the effects included in the complex speed of wave propagation must be considered — namely, the viscous fluid effects. For such sensors, of a size on the order of $L_0 = 0.25$ cm and of correspondingly small thickness, significant departures from $f_n = kT^{1/2}$ have been observed.

The speed of wave propagation in a duct or similarly confined area may be expressed approximately as [2]

$$|c|^4 = \frac{a^4}{1 + \frac{R_r^2}{\omega^2 L_i^2}} \tag{12}$$

where

R_r = resistance per unit length of the propagation path,

L_i = the inertance per unit length of the propagation path, and

ω = the angular frequency of the signal, that is, $\omega = 2\pi f$.

The resistance is dependent upon the fluid viscosity μ and cross-sectional area A:

$$R_r = k_1 \frac{\mu}{A^2} .$$

The inertance is dependent upon the fluid density ρ and the cross-sectional area:

---

* In some applications these extreme conditions may be encountered, in which case the γR product can be determined experimentally.

$$L_i = k_2 \frac{\rho}{A} .$$

k_1 and k_2 are constants, dependent upon the geometry of the duct or cavity. Making substitutions in equation 12:

$$|c|^4 = \frac{a^4}{1 + k_3 \dfrac{\mu^2}{f^2 \rho^2 A}} \tag{13}$$

Now for $c \simeq a$, we must have

$$k_3 \frac{\mu^2}{f^2 \rho^2 A^2} \ll 1$$

More specifically, viscosity, frequency, and density are all to some degree dependent upon temperature. Thus, it is apparent that the overall dependence of a on temperature will be changed —that is,

$$f_n \neq k T^{1/2}$$

Also, density is a function of input pressure as well as temperature. This in conjunction with the area A (a nontemperature—dependent quantity) effects additional changes in the value of k.

In view of the foregoing statements, it becomes convenient from an experimental standpoint to represent output frequency as

$$f_{out} = k T^{\alpha},$$

where α is approximately constant for temperature ranges that are not extremely large,

$$1/2 \geq \alpha > 0;$$

and sensitivity as

$$\frac{df_{out}}{dT} = \alpha k T^{\alpha - 1} = K_s T^{-\beta} \tag{14}$$

Values for α and k for a certain range of temperature can be determined with relative ease from a log-log plot of output frequency versus temperature as shown in figure 34. Given any two points on the curve yields α from the equation

$$\alpha = \frac{\log f_2 - \log f_1}{\log T_2 - \log T_1}; \tag{15}$$

then,

$$k = \frac{f_1}{T_1^{\alpha}} = \frac{f_2}{T_2^{\alpha}} \tag{16}$$

k can also be read directly from the f_{out} versus T plot by extrapolating the curve to T = 1. At this point,

$$f_{out} = k(T)^{\alpha} = K.$$

From the above, sensitivity at any point is determined by equation (14).

A typical plot of sensitivity is shown in figure 35.

3.1.6   Temperature Range

3.1.6.1 Operational Factors

It has been shown in the previous sections that the range of temperatures encountered can be expected to influence sensor performance. Specifically, as temperatures get higher, sensitivity and signal amplitude decrease; threshold input pressure and signal-isolation ratio increase; and the specific heat ratio and gas constant may no longer be constants. Notwithstanding, it has been possible in all cases to date to successfully integrate these performance characteristics into a suitable design for a given application.

A knowledge of the flow field in which the temperature is to be measured is necessary for a successful flueric sensor application. When the pressure and temperature of the flow field are grossly different from the standard conditions, the flow process may depart significantly from behavior as predicted by flow equations based on the assumption of a perfect gas. Jordan and Mintz have generated tables of the compressible flow functions for air over a large range of temperatures and pressures. Figures 36 through 39 (extracted from reference 3) illustrate the departure from perfect gas behavior for two typical flow functions at Mach numbers of one and two; $p/p°$ is the ratio of static pressure to stagnation pressure, and $T/T°$ is the ratio of static temperature to stagnation temperature.

Analytically, it is possible to show—based on the complex speed of wave propagation—that at some temperature T_1 a maximum exists in the frequency-versus-temperature curve. At this point,

$$\frac{df_{out}}{dT} = \frac{df_{out}}{dT_1} = 0.$$

Thus, in the vicinity of T_1 the sensor is relatively insensitive to temperature changes; and for $T > T$ df/dt is negative. This condition will exist at a unique temperature, dependent upon signal frequency and acoustic path cross-sectional area. However, experimental evidence indicates that no such condition exists for sensors of the present miniature design, for temperatures well above the endurance limit of known usable materials.

3.1.6.2 Materials

The upper temperature limit for the flueric temperature sensor is currently determined by the material from which the sensor is fabricated. There appear to be few workable materials that will give

satisfactory service at sustained temperatures in excess of 1000°K (727°C). Although this is well below the melting point of quite a few materials, the environment to which most sensors are exposed produces a serious problem of oxidation at these temperatures. The material loss and the accompanying dimensional changes due to oxidation may not of themselves be serious; it is the blockage of the small nozzles in miniature sensors by the dislodged oxidized material that creates the problem. Even in nonoxidizing environments, the chemical and physical changes that occur with some of the high-melting-point materials render them undersirable.

The selection of a suitable material for a given temperature range is made more complicated by the fact that the available specifications for the material may apply to a less severe environment than that for the design environment. For example, a material rated as having a low rate of oxidation at a given temperature in a zero-velocity environment may oxidize at an unsatisfactorily high rate at the same or lower temperature in a high velocity environment, because the oxygen in the near vicinity of the material is being continually replenished by the flow. Such was the experience during tests with a sensor constructed of 310 stainless steel. This particular stainless steel is said to have high resistance to scaling for continuous service at temperatures up to 1420°K. The sensor was operated for approximately 8 hr between 300° and 1180°K, and for approximately 4 hr at 1180 K. The sensor under these test conditions was supplied with air that had passed through a heating coil constructed of 310 stainless steel. Scaling in the heating coil was of such magnitude as to render the sensor inoperative on several of the tests. Figure 40 shows a sample of the residue retrieved from the heating coil.

3.1.7   Response Time

The response time of a temperature-measuring device becomes a highly important performance characteristic for certain applications. Such an application is in the control of the fuel flow of a turbine engine, where fuel-flow control is dependent upon gas temperature, and flow corrections must be made in a minimum time. For this type of application, the response time of conventional measurement systems is considered undersirably long; and as the temperature range becomes higher, the response time becomes longer.

The response time is defined as the time $t = \tau$ required for the sensor to change frequency by 67 percent of the final frequency change effected by the step change in temperature. The significance of sensor material selection is again manifested in that it is of distinct advantage to have a material of low-mass density and high-thermal conductivity; also, fabrication techniques that allow a minimum total mass of material become important for response time considerations.

Perhaps the most readily recognized prerequisite for a short response time is a short cavity sweep-out time — that is, the time required to flush the cavity of fluid at temperature T_1 and replace it with fluid at temperature T_2. This sweep-out time depends on several factors:

     (1) Cavity volume;

     (2) Cavity shape;

22

(3)   Internal flow velocity; and

(4)   Mixing characteristics of the flow.

At present, very little has been done on specific studies of response time; however, design features that are favorable to good response time have been incorporated in sensors for certain applications with satisfactory results.

Where the system response time is a critical factor, the signal transport time must be considered. Therefore, the transmission distance should be as short as is feasible. Some observations have indicated still other considerations with respect to signal transmission. When the transmission line is long and the signal pressure tap is small, essentially a large capacitance is connected to the sensor cavity by an orifice. If the sensor input pressure is changed rather rapidly, a significant period of time may be required for the transmission line to reach the new steady-state pressure. During the transition, signal frequency and amplitude are inaccurate; thus, response time must include this period. The problem can generally be alleviated by increasing the size of the pressure tap and/or decreasing the volume of the transmission line.

3.2   Other Design Considerations

Some very important non-performance factors must also be considered in sensor design. These factors include service environment and application considerations. The service environment and the application receive primary consideration when specific output characteristics are required, and when precautions must be taken to protect the sensor and its operation from the environment.

3.2.1   Nature of Environment

The nature of the flow environment must be known for three reasons:

(1)   To insure that the desired output signal is produced in the specified environment;

(2)   To employ appropriate design and fabrication techniques so that the sensor might be protected from likely hazards such as particle contaminated gases and radiation; and

(3)   So that the gas characteristics (γ and R) may be used to calibrate the sensor.

3.2.2   Size and Shape

In general, the temperature of a fluid stream can be measured more accurately if the sensor can be placed directly in the stream. When this is done, small size and specified shape are extremely important. In cases where a specific system requires a low-frequency output, a large sensor may be required.*

---

*Low-frequency outputs may also be obtained by employing two sensors and a beat-frequency technique.

Oscillators with internal-geometry planform areas varying from several square centimeters to less than 0.3 cm^2 have been designed from the performance curves previously shown. When a particular oscillator is desired in a size different from a present design, the dimension L_0 is usually selected first, according to the requirements of the new application; the h/L and b/L ratios are then used for scaling.

The effect of the size of the sensor on performance has been discussed previously. Generally, it may be stated that the miniaturization of flueric temperature sensors is presently limited only by fabrication techniques.

3.2.3 System Requirements

The temperature sensor is never used as an independent device. When the sensor is used for measurement only a transmission line and transducer are required. The transmission line is necessary to communicate the signal to the transducer, which must necessarily be outside the extreme temperature environment. When the sensor is used in a flueric temperature measurement and control system, a transducer, transmission lines, and various other matched flueric elements are required. It can be seen that the major system requirements are those associated with transmission lines, transducers, and the matching of components.

The problems associated with signal transmission are attenuation and distortion. These problems can usually be minimized by careful transmission-line design. Basic practices that have been used successfully are to:

(a) Choose a line less than one-sixth of a wave length in diameter.

(b) Extend, when possible, the transmission line past the transducer; or terminate it properly to reduce or eliminate reflected waves.

(c) Keep the lines as short as possible within the above restriction.

(d) Avoid changes in cross section where possible.

The average transducer with a resonant frequency of 100 kHz is satisfactory when the fundamental frequency of the sensor is below 20 kHz. When the fundamental frequency is above 20 kHz, particularly above 25 kHz, the higher harmonics may resonate the crystal. The third (and higher when present) harmonic is in the resonance range of the average transducer and can cause severe signal distortion and erroneous frequency readings. For monitoring with a fundamental frequency above 25 kHz, transducers with a resonant frequency appreciably above 100 kHz should be used.

In general, the signal from the sensor cannot be applied directly to a proportional amplifier(converter) in a proportional temperature control system. The output frequency of most sensors is considerably higher than the frequency response of most amplifiers. A reference

oscillator, decouplers, and a mixer are used to produce a difference
frequency which is within the response range of the amplifier. Matching
in this type of system refers to matching the frequency and amplitude
of the output signal from the mixer to the input requirements of the
amplifier.

3.2.4   Fabrication

As stated, the flueric temperature sensor is limited in high-temper-
ature-measurement capability only by the limitations of the case material.
Since the sensor is usually made in two or more parts, a means of joining
the parts is required. This process must provide a leak-free seal and
must withstand the stresses imposed by the service environment.

Diffusion bonding seems to be an ideal joining process for tem-
perature sensor parts. It eliminates the assembly stresses generated by
bolting or riveting. Service stresses are evenly distributed across the
total bonded area rather than concentrated at bolts or rivets. Diffusion
bonding can be achieved without changing the heat-treated condition of
the metal. Since no low-temperature alloys are involved (as in brazing),
diffusion bonded joints can withstand operating temperatures equal to the
temperature resistance of the parent metal.

Chemically clean and extremely fine surface finishes and special
fixtures are required to achieve high-quality diffusion bonding. Once
the techniques are developed, it should be possible to achieve good bonds
repeatedly with minimum difficulty. The state-of-the-art of diffusion
bonding is covered in the literature [5], [6], [7].

The selection of sensor material depends primarily on the service
environment. Materials must be selected for specific applications. Free-
machining materials like brass, aluminum and filled epoxies have been used
most often for research work at HDL. For temperatures above 800°K (527°C),
stainless steel has been used; however, the oxidation resistance was not
what was expected (see sect 3.1.6).

Fabrication processes other than conventional machining have been
investigated. Individual sensors and systems produced by photoetching
a plastic material have functioned satisfactorily. Some difficulty was
encountered with obtaining the full depth of the etch in the throat of
small nozzles (on the order of 0.25 mm).

Presently, castable ceramic materials are being considered for
applications where the sensor is not subjected to severe thermal shock.
The cast parts would be bonded together with a high-temperature cement.
The combination would be rated for use at approximately 1700°K (1427°C).
Nickel-chromium alloys appear to hold greatest promise in the immediate
future for high-temperature oxidation resistance. Some of these materials
should be satisfactory at temperatures up to 1700°K (1427°C); and some
chrome composites may be satisfactory for limited use to 1900°K (1627°C).

3.3   Design Approach

The approach employed in a specific sensor design is dictated
by the characteristics of the fluid medium in which the temperature is

to be measured. Where possible, the sensor is immersed in the fluid. The flow-field characterics that should be known before initiating the design are as follows:

(1) Static pressure,

(2) Stagnation pressure,

(3) Temperature range,

(4) Type of gas (γ, R, chemical composition), and

(5) Sensor volume or frontal area that the stream can tolerate.

The flow-field characteristics are significant for the following reasons:

(1) The static-to-stagnation pressure ratio will determine the required threshold and whether choked flow can be achieved in the outlet nozzle.

(2) The temperature range (or variation) will determine the desired sensitivity, and initially determine the sensor material.

(3) The ratio of specific heats and the gas constant (γ and R) will determine the sensitivity as related to the gas.

(4) The chemical composition of the fluid will affect material selection.

(5) The size of the flow field will determine the size of sensor that may be used without introducing significant measurement errors.

In general, if a sensor has the required threshold and sensitivity, all other characterisitics are satisfactory. The following would be a normal design procedure:

(1) Select a value of L_0 that gives the desired sensitivity, or that which is compatible with the size of the flow field —whichever is most limiting.

(2) Select a value of h/L_0 or b/L_0 that yields the required threshold.

(3) Determine the value of the ratio not chosen in (2) from figure 41 that gives the relationship between b/L_0 and h/L_0.

4.   APPLICATIONS

A number of flueric temperature sensor application studies have been conducted. In general, the studies were performed for the purpose of applying the sensor to the measurement of stagnation temperature in fluid streams. In most applications considered, the requirement was to measure high steady-state temperatures and high-temperature transients of short duration. Although sensors can be designed in a size and shape for broad general use, the usual approach has been to study each sensor application separately. The practice of designing sensors for broad

26

application will undoubtably be adopted when more is known about the measurement environments and ideal sensor materials have been selected.

5.   CONCLUDING REMARKS

The state-of-the-art in flueric temperature design makes possible the design of sensors for a variety of applications, and these designs can be realized with greater predictability than was previously the case.   This improved design capability is primarily the result of an experimental research effort, since the theoretical analyses have been somewhat limited in scope.

In future programs at HDL greater emphasis is anticipated on the theoretical aspect of the analysis of the basic phenomena present in these devices.

Much of the future of flueric temperature sensors will depend upon the materials to meet the temperature requirements, and the fabrication methods to allow reduction in overall size and total mass.   Although there are limitations in these areas at present, the outlook is promising.

Much remains to be done if routine application of flueric oscillators to temperature measurement is to be realized.   The purpose here has been to provide information that will to some extent stimulate applications and innovations which, in turn, will provide a stronger impetus to advancement in this area of temperature sensing.

6.   LITERATURE CITED

[1] Brown, G. B., "The Vortex Motion Causing Edgetones," Proc Phys. Soc (London), Vol 49, p 493 (1937).

[2] Kirshner, Joseph M. (Editor), Fluid Amplifiers, McGraw-Hill, New York, p 175, 1966.

[3] Jordan, Duane P., and Mintz, Michael D., Air Tables, McGaw-Hill, New York, 1965.

[4] Gottron, Richard N. and Gaylord, Wilmer, "A Temperature Control System Using Flueric Components," Proceedings of the Fluid Amplification Symposium, October 1965, Vol. III, Harry Diamond Laboratories, Washington, D. C. 20438.

[5] Solar (Div. of International Harvester Co), San Diego, Calif., "Final Report on Diffusion Bonding of Refractory Metals and TD Nickel," AFML-TR-64-394 (Project 7-935), Air Force Materials Laboratory, Air Force Systems Commands, Wright-Patterson Air Force Base, Ohio, December 1964.

[6] Garrett, B.R., Blank, G. F., and Ranadive, A. J. (Haxel Products, Inc., Berkeley, Calif.), "Broad Applications of Diffusion Bonding," NASA CR-409 (Contract No. NAS 7-273), NASA, Washington, D. C., March 1966.

[7] Kammer, P.A. and Hauser, D., (Battelle Memorial-Institute) "Surface-Layer Bonding," Paper No. III-3, Society of Aerospace Materials and Process Engineers, 9th National Symposium ("Joining of Materials for Aerospace Systems"), 15, 16, 17 November 1965, Dayton, Ohio.

NOMENCLATURE

A_{ap}	cross-sectional area of acoustic path
A_i	area of the sensor input nozzle
A_e	area of the sensor exhaust nozzle
a	speed of sound; free air conditions
(a)	absolute pressure; e. g.,kN/m^2 (a)
α	exponent used in relating temperature to the output frequency of the sensor
b	width (or breadth) of cavity
c	complex speed of wave propagation
γ	ratio of specific heats for a gas
e	correction to acoustic path length for the effect of radiation from open end of resonant cavity
f_n	resonant frequency of cavity; n = 1, 2, 3...
f_{out}	output frequency of operating sensor
(g)	gage pressure; e. g., kN/m^2 (g)
h	distance from input nozzle exit to edge of splitter (splitter distance)
j	constant determined by mode of jet oscillation
k_n	arbitrary constant; n = 1, 2, 3...
K	constant relating temperature to the output frequency of sensor
L	acoustic path length
ℓ	length of cavity
L_i	fluid inertance
μ	viscosity of fluid
m_n	slope of a straight-line curve; n = 1, 2, 3...
n	denotes positive consecutive integers
P_{out}	output signal amplitude; peak-to-peak pressure
p_i	total pressure at the upstream side of the input nozzle
p_{i_t}	input pressure at threshold of operation
p_c	cavity steady-state pressure

p_e	pressure to which sensor exhausts
R	gas constant
R_r	fluid resistance
ρ	mass density
Si	signal-isolation ratio
S_t	switching time
T	absolute temperature
t	thickness (or depth) of sensor
τ	response time of sensor
u	velocity of jet
w_i	width of input nozzle
w_e	width of exhaust nozzle
w_s	width of splitter at the stream-wise leading edge
ω	angular frequency
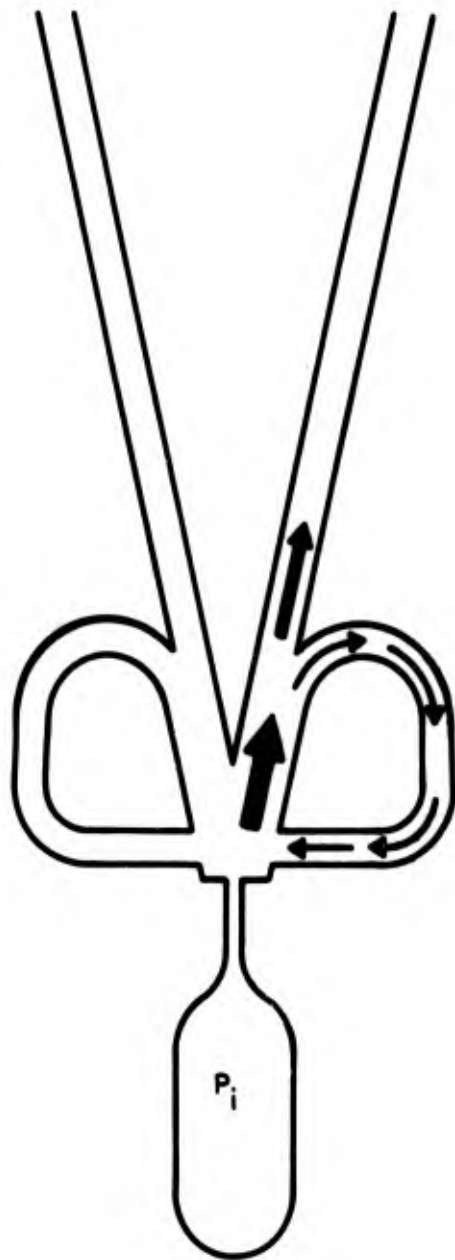
Figure 1. Feedback oscillator
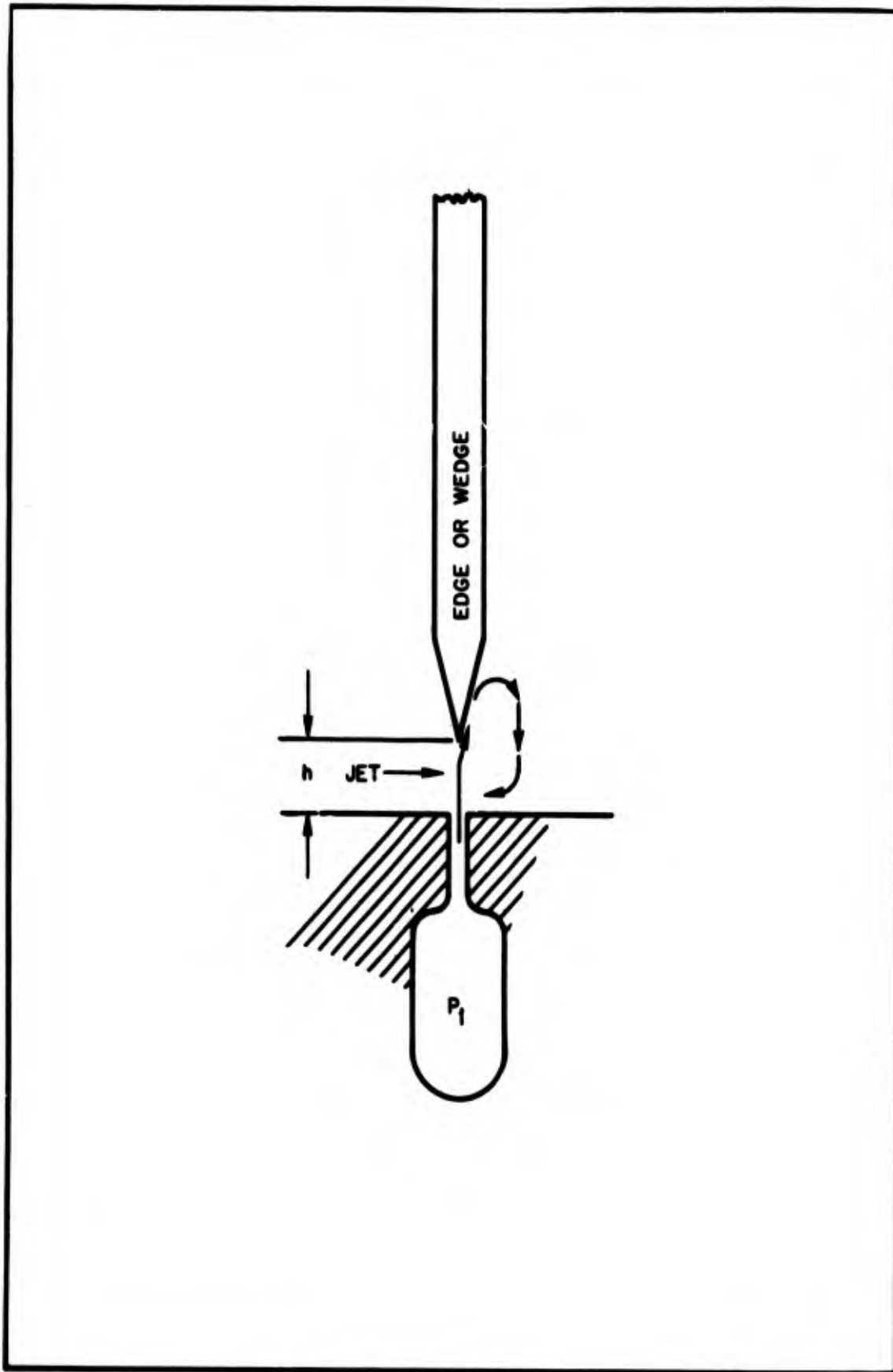
Figure 2. Jet-edge system.
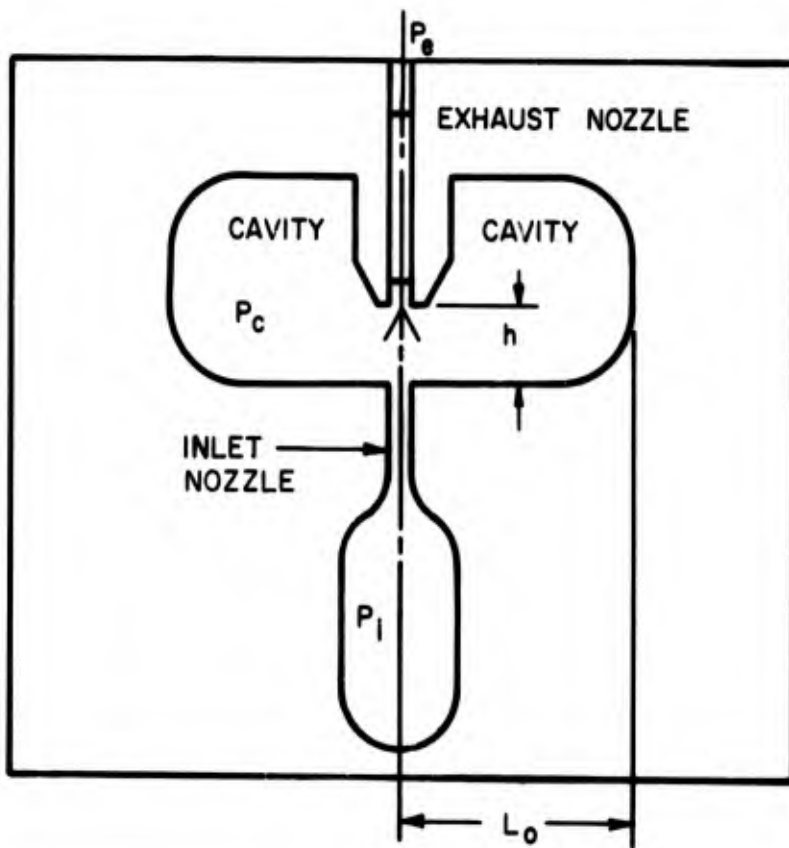
Figure 3. Jet-edge resonator oscillator.
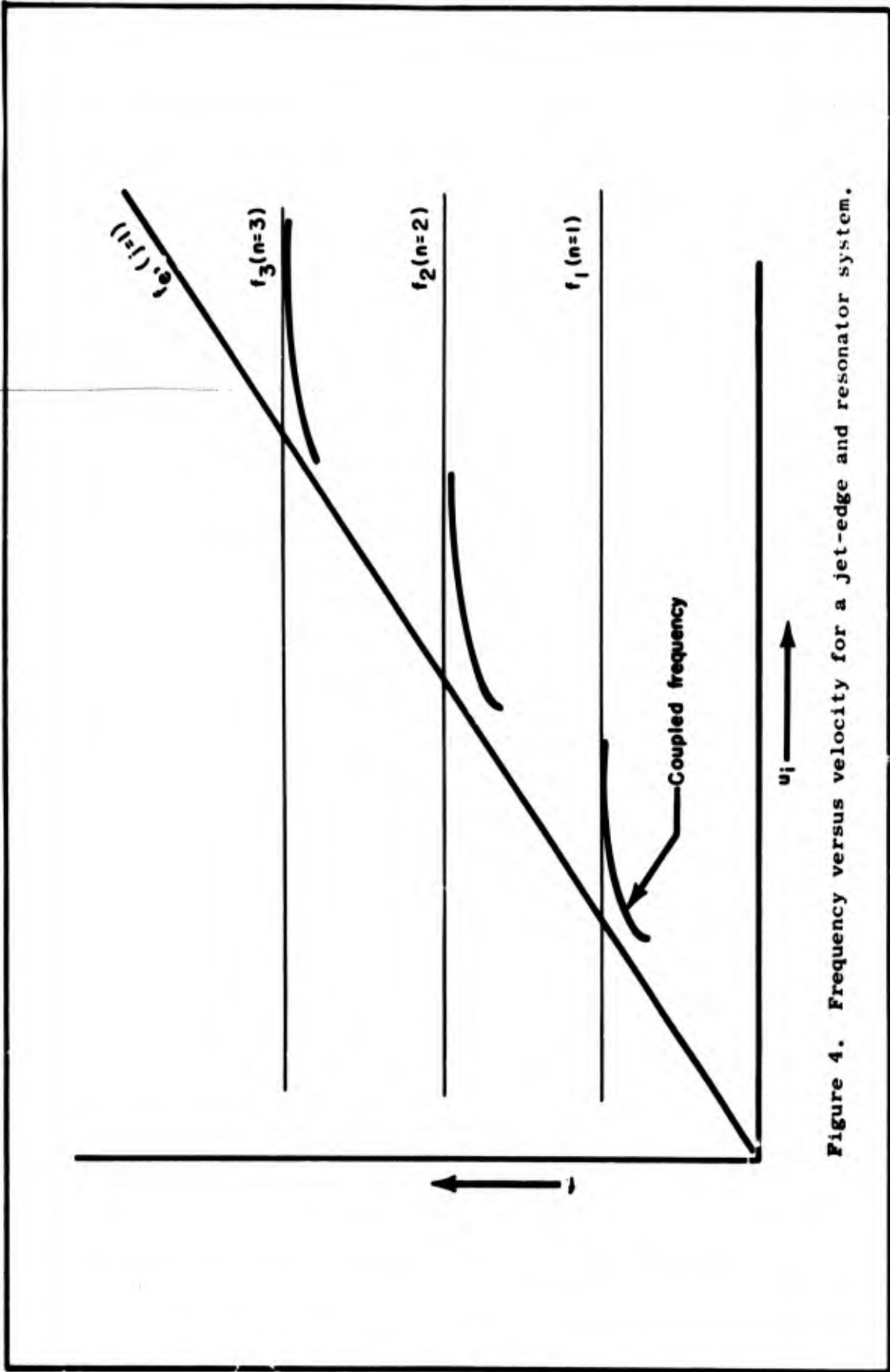
Figure 4. Frequency versus velocity for a jet-edge and resonator system.
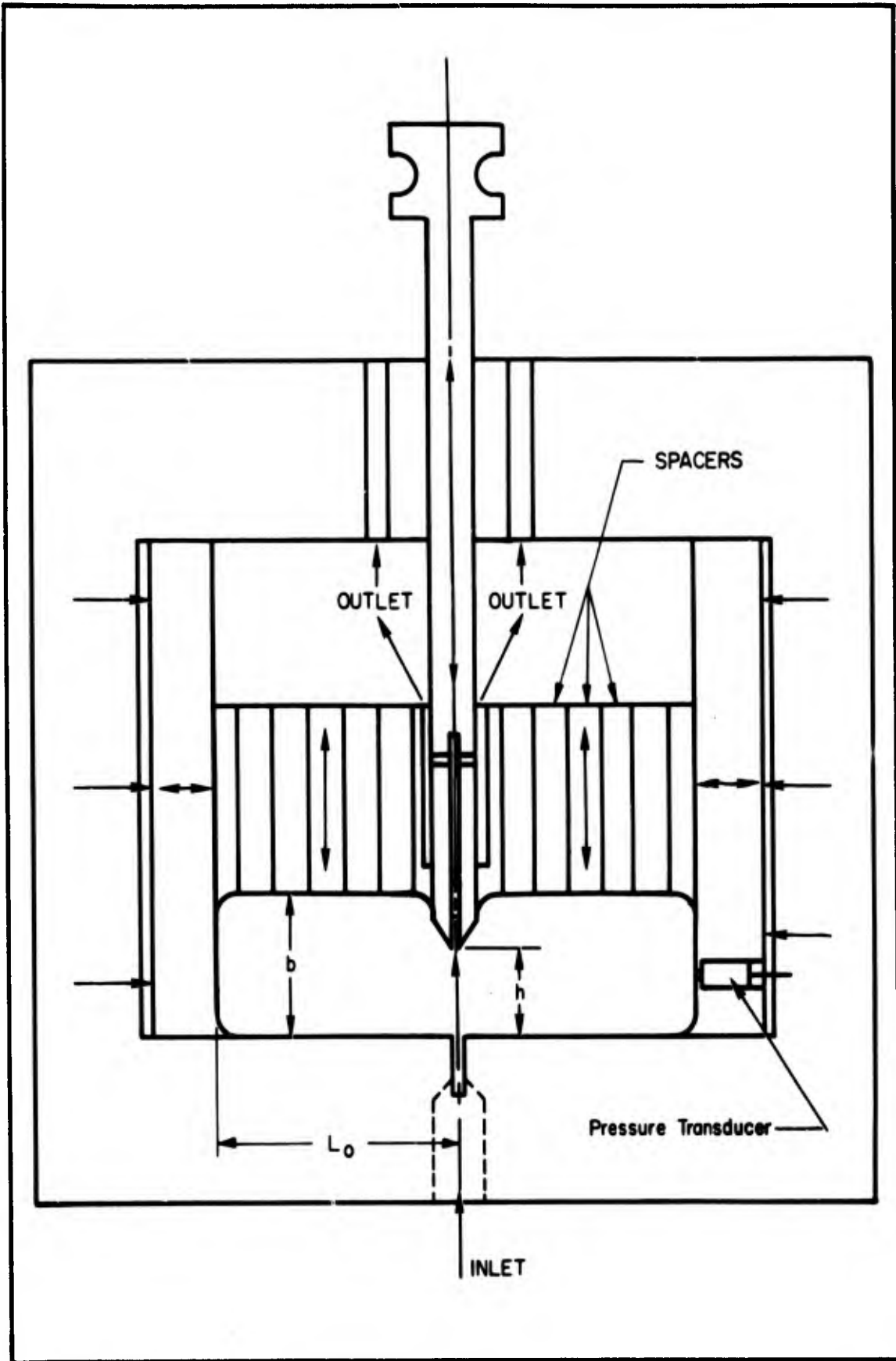
Figure 5. Diagram of experimental oscillator.
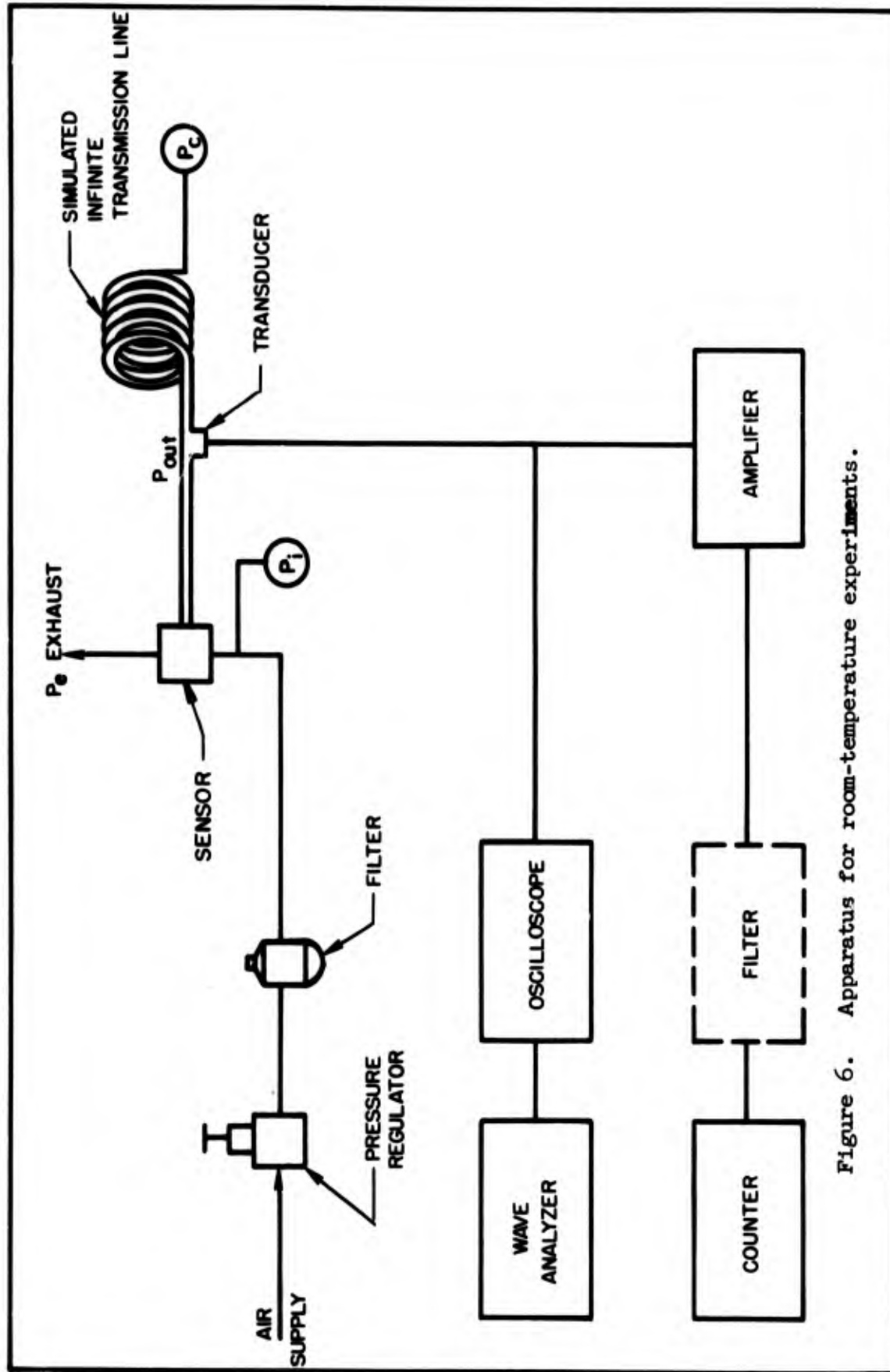
Figure 6. Apparatus for room-temperature experiments.
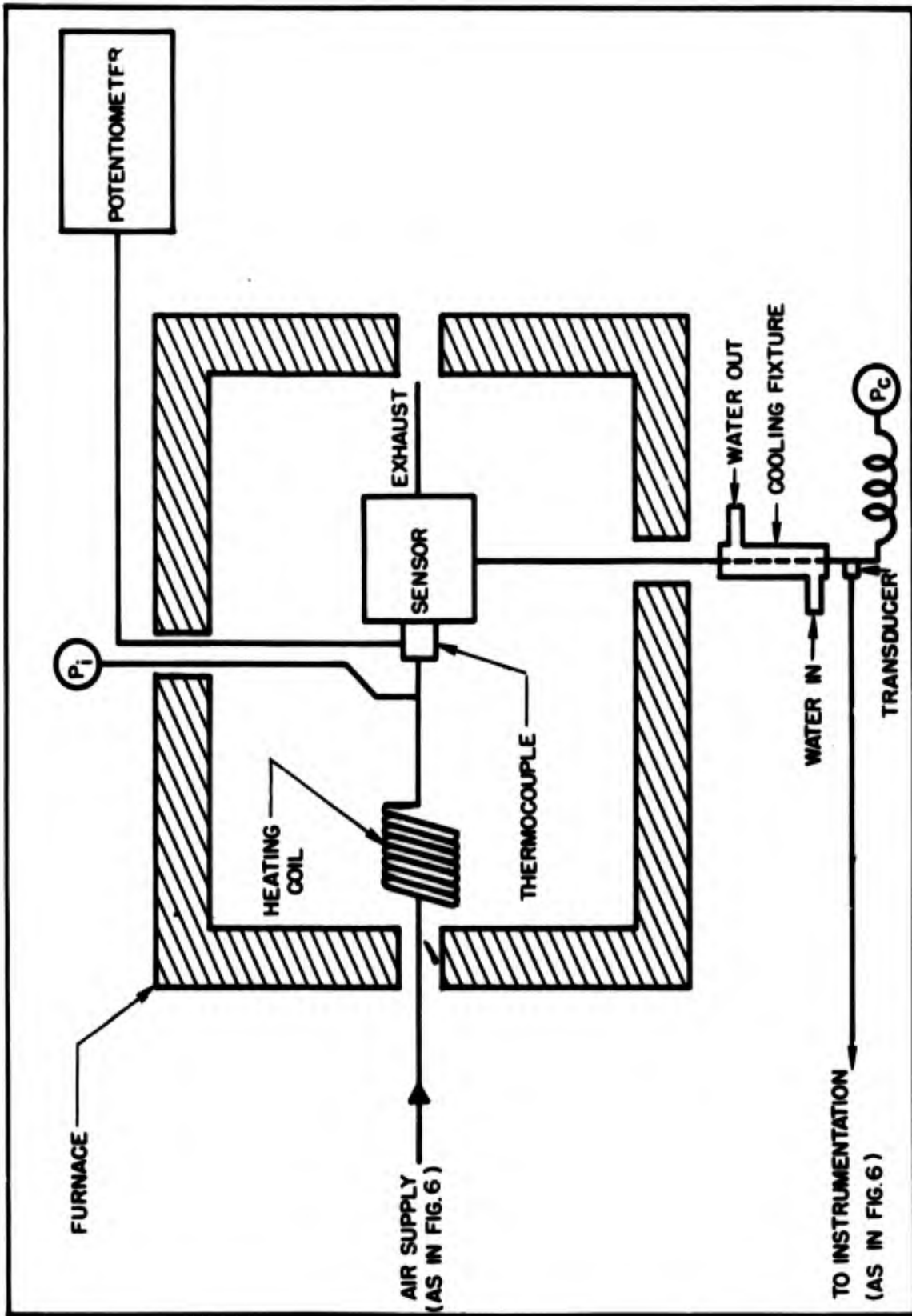
Figure 7. Apparatus for conducting experiments at elevated temperatures and for temperature calibration.

37
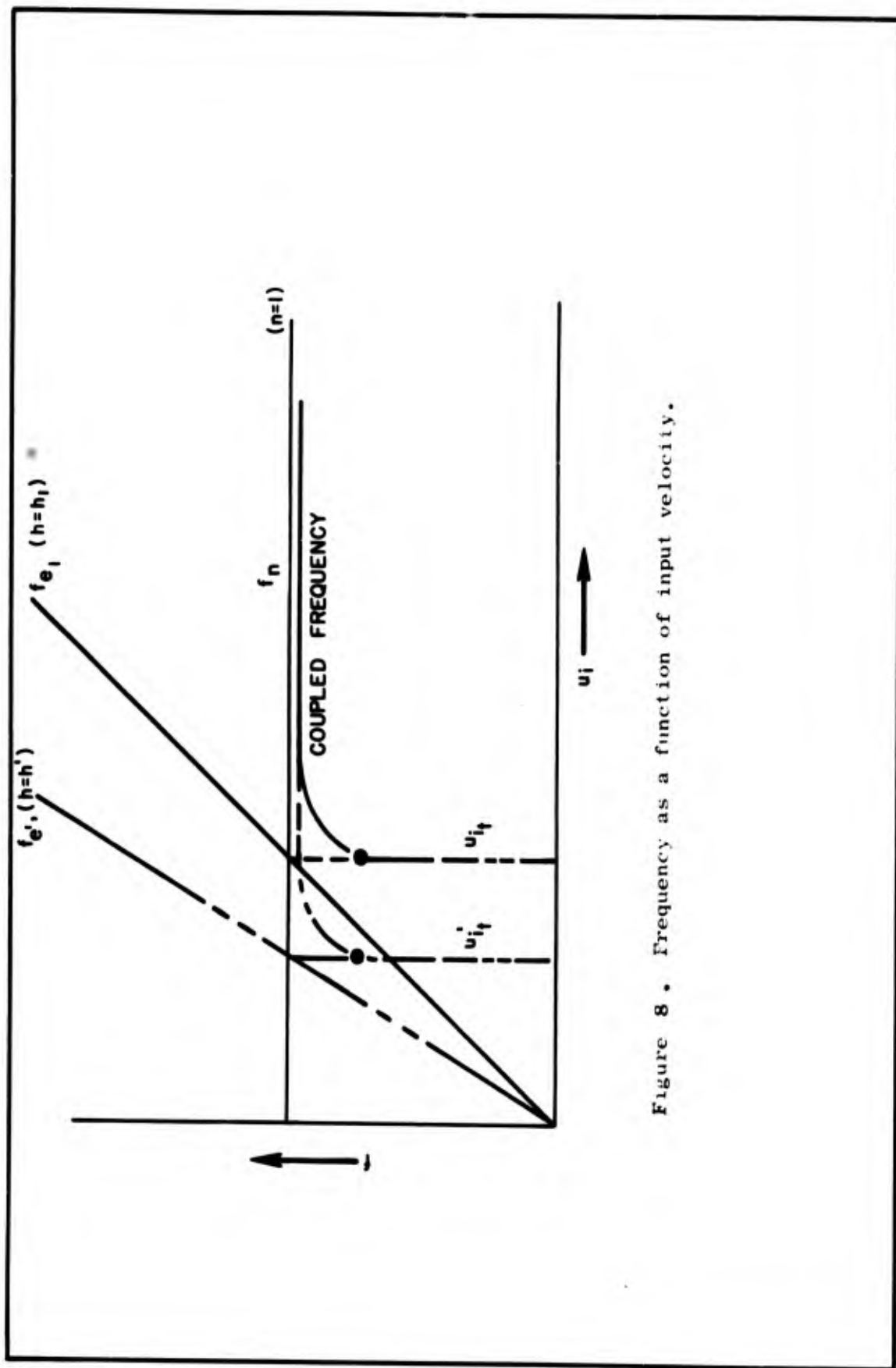
Figure 8. Frequency as a function of input velocity.
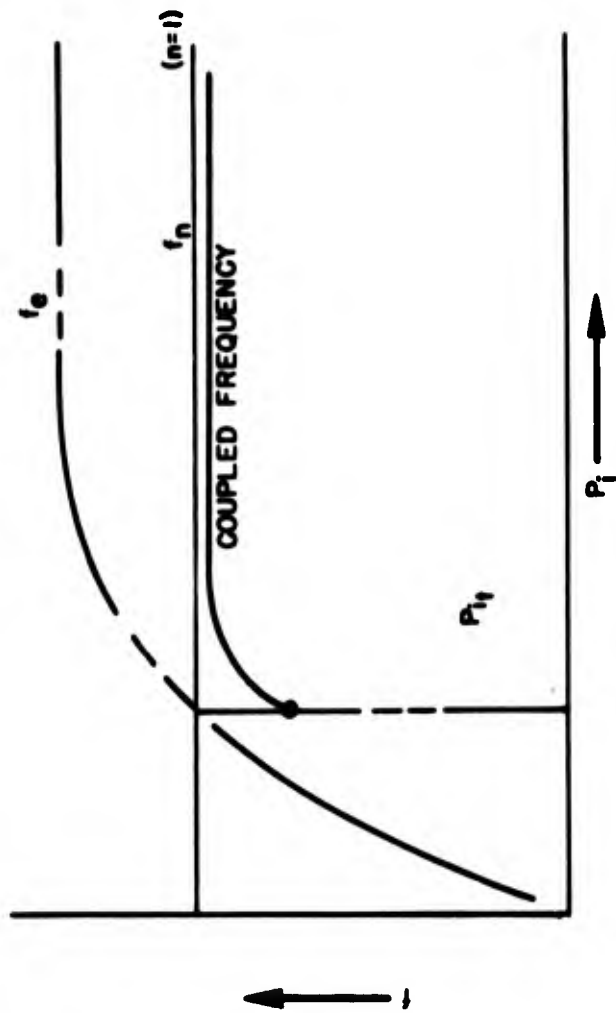
Figure 9. Frequency as a function of input pressure.
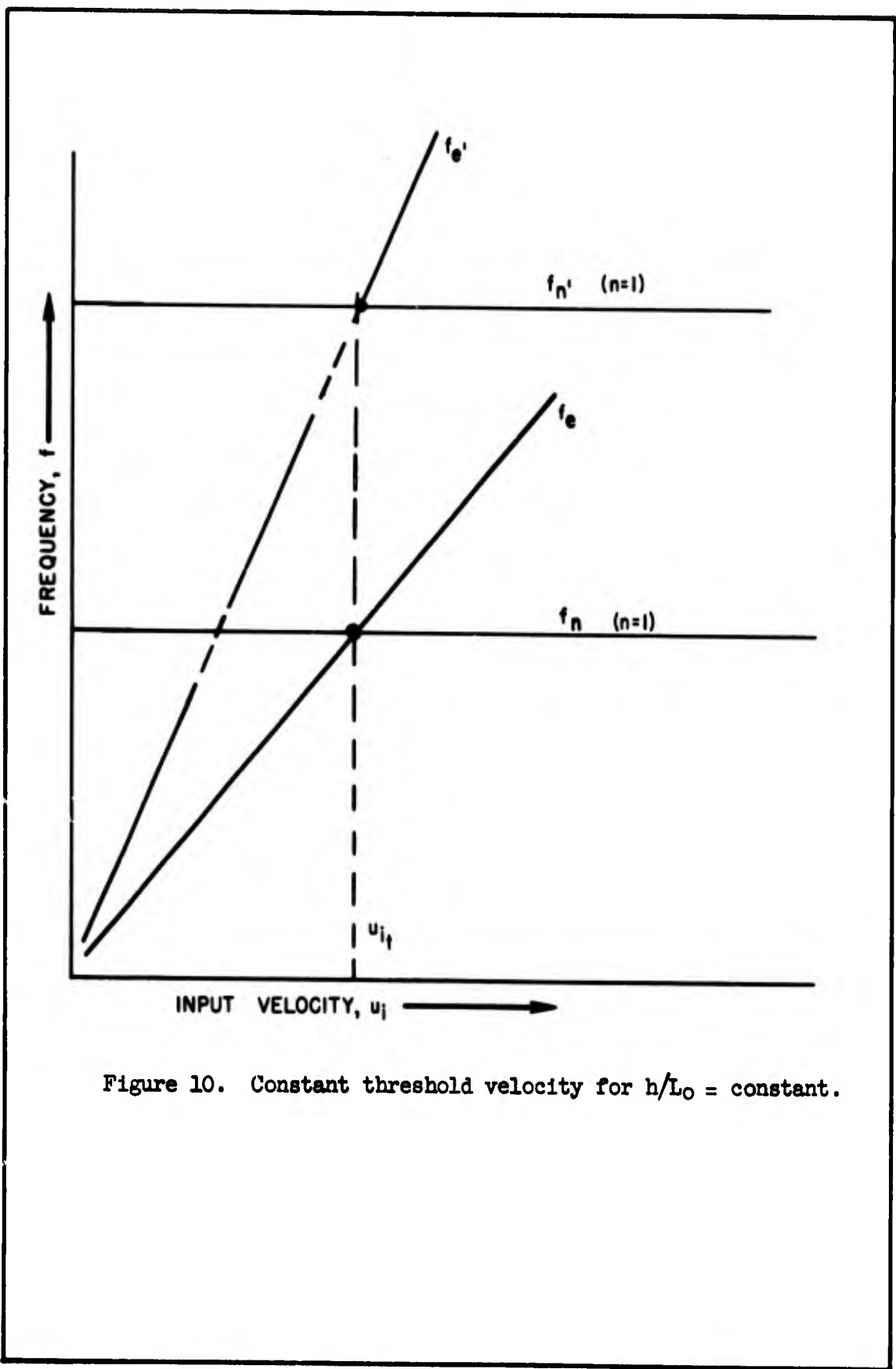
Figure 10. Constant threshold velocity for h/L_O = constant.

Figure 11. Threshold pressure versus breadth.
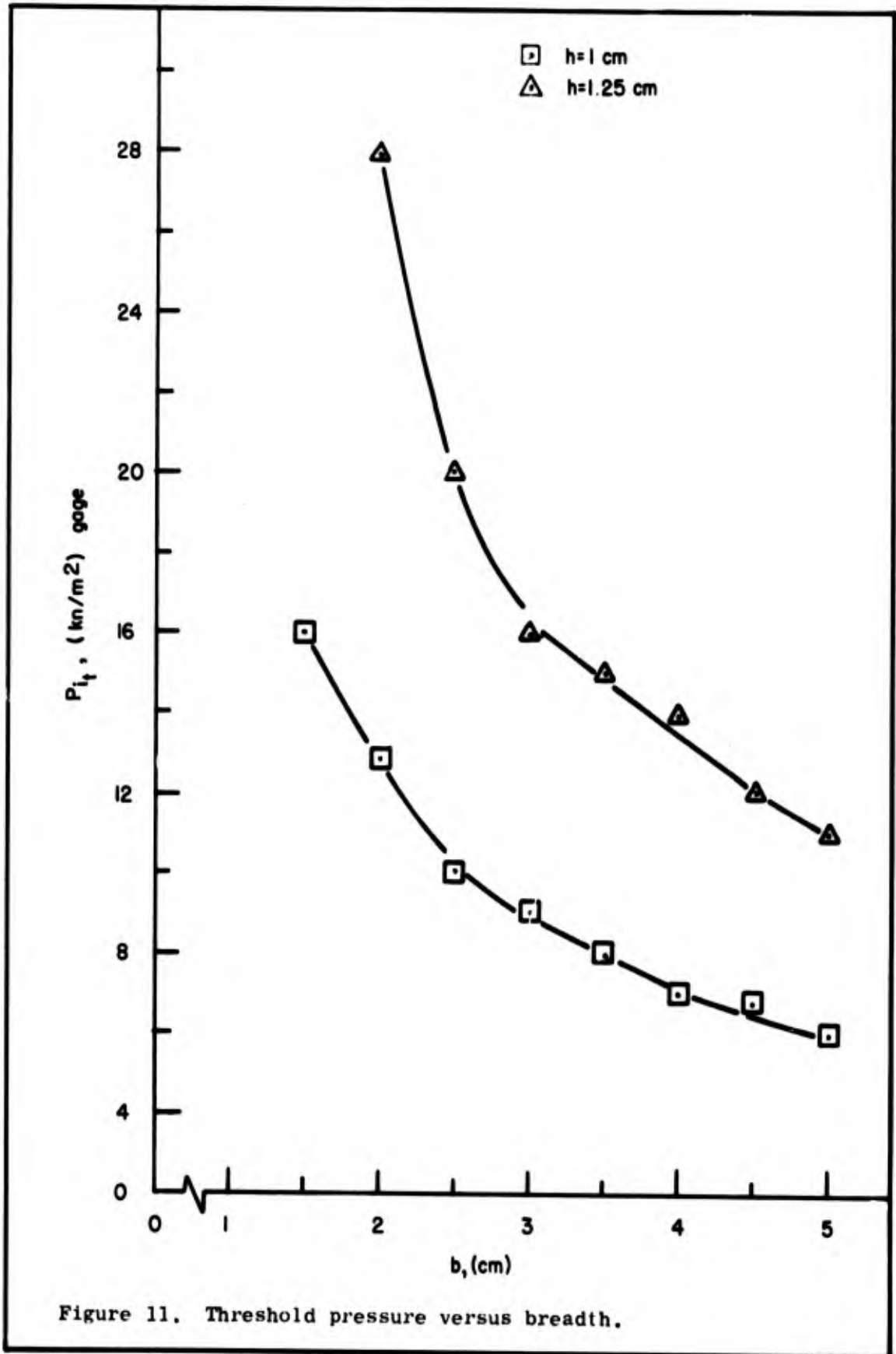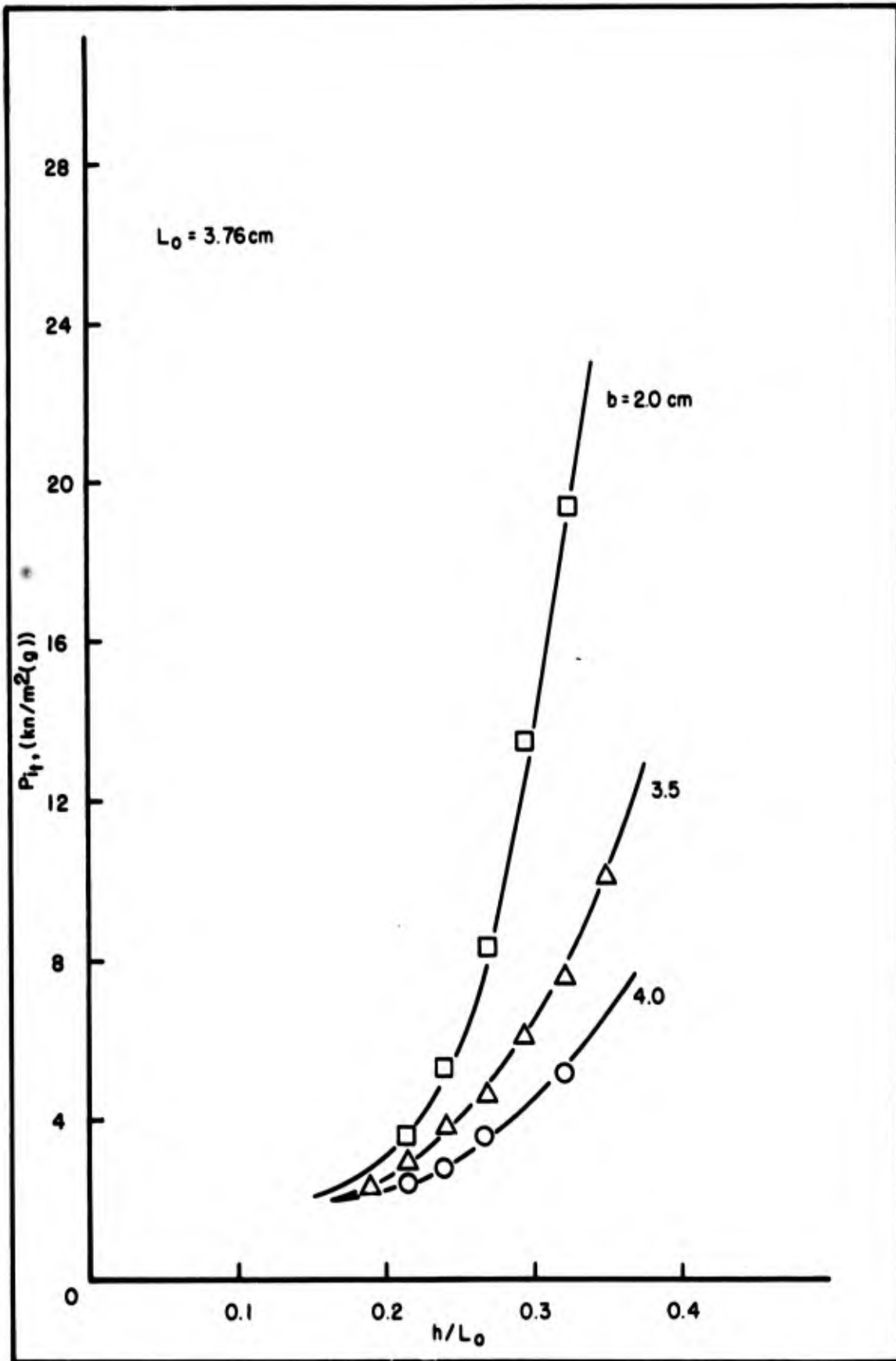
Figure 12. P_{i_t} versus h/L_o for three values of b.
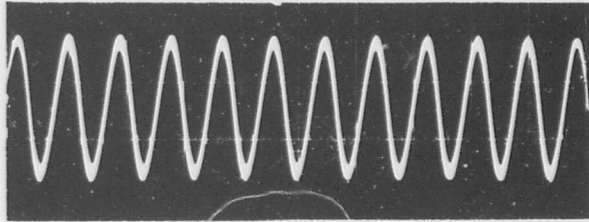
$T = 298°\,K$
$P_i = 350\,kn/m^2\,(g)$
$f_{out} = 22{,}080\;Hz$
$P_{out} = 9.3\;kn/m^2$
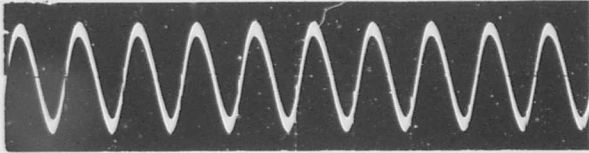
$T \approx 298°\,K$
$P_i = 50\,kn/m^2\,(g)$
$f_{out} = 21{,}244\;Hz$
$P_{out} = 7.34\;kn/m^2$
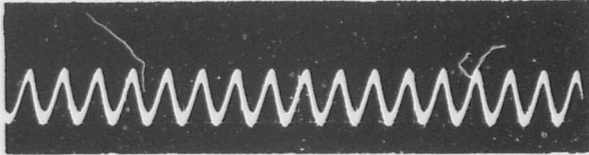
$T = 684°\,K$
$P_i = 350\,kn/m^2\,(g)$
$f_{out} = 32{,}899\;Hz$
$P_{out} = 3.72\;kn/m^2$
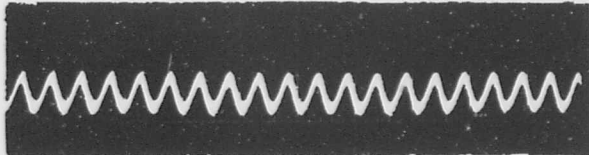
$T = 942°\,K$
$P_i = 350\,kn/m^2\,(g)$
$f_{out} = 38{,}329\;Hz$
$P_{out} = 3.64\;kn/m^2$
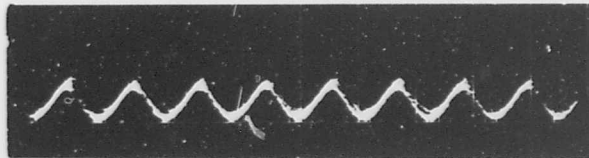
$T = 1181°\,K$
$P_i = 350\,kn/m^2\,(g)$
$f_{out} = 42{,}633\;Hz$
$P_{out} = 1.86\;kn/m^2$

Figure 13.   Typical oscillator signals.
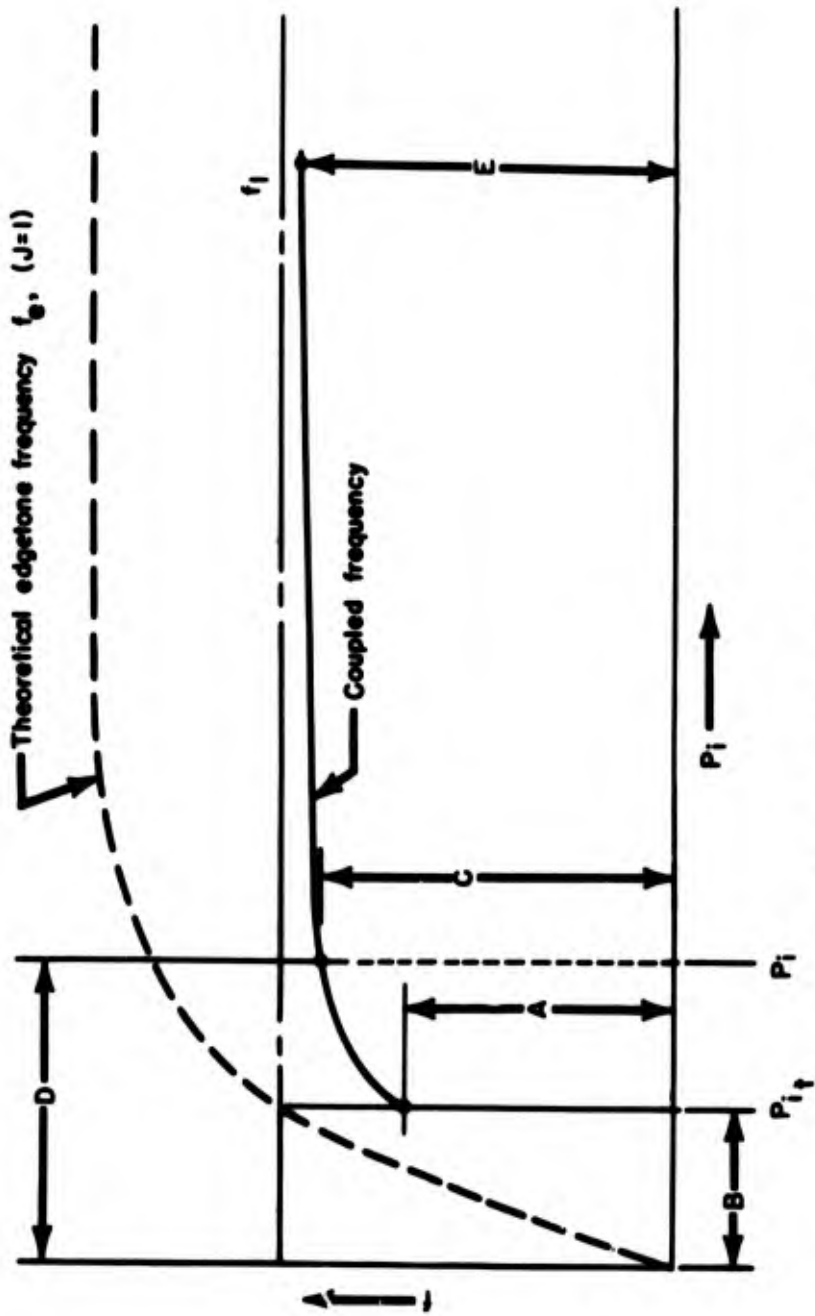
Figure 14. Significant areas in coupling.
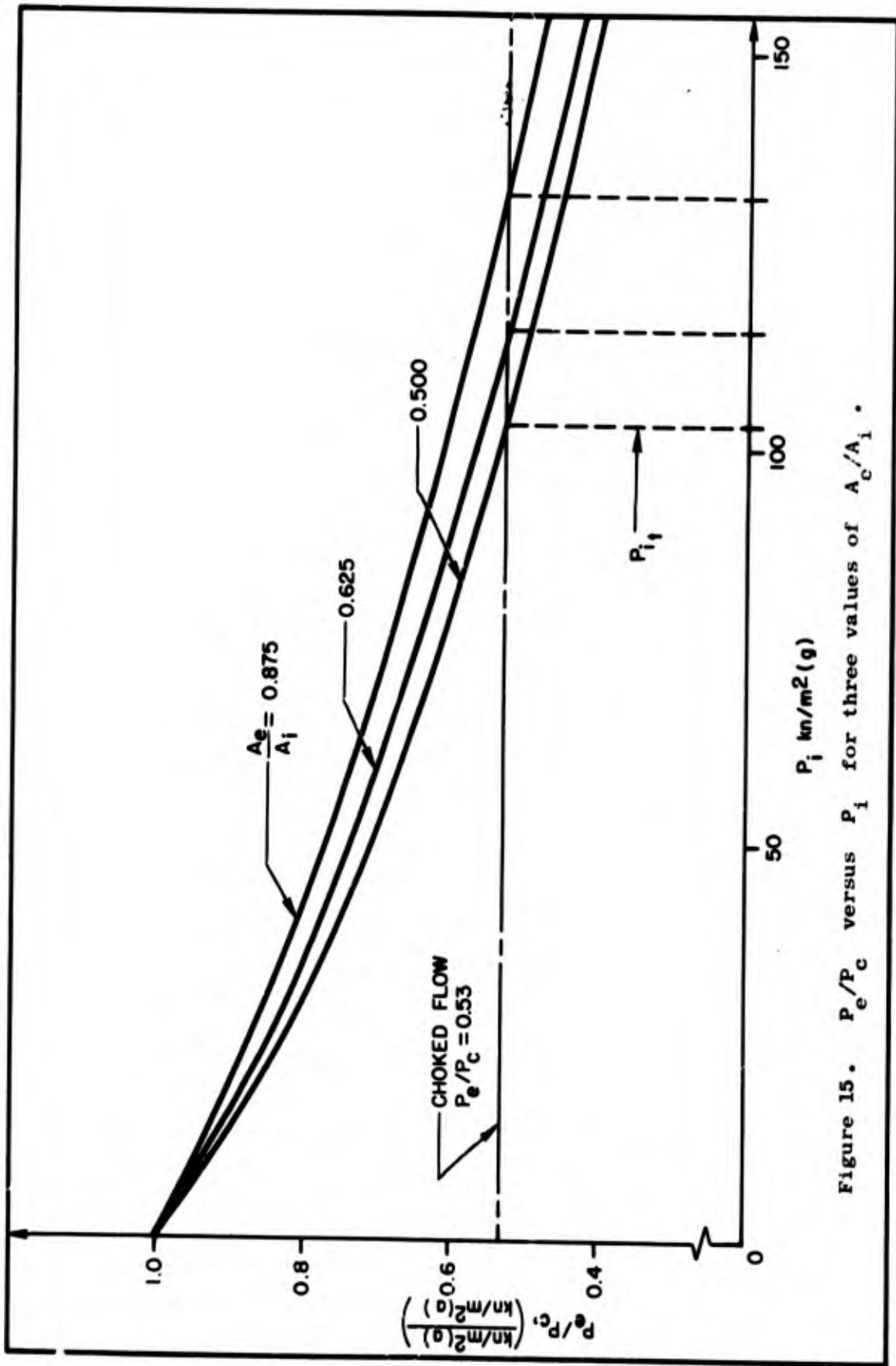
Figure 15. P_e/P_c versus P_i for three values of A_c/A_i.

45
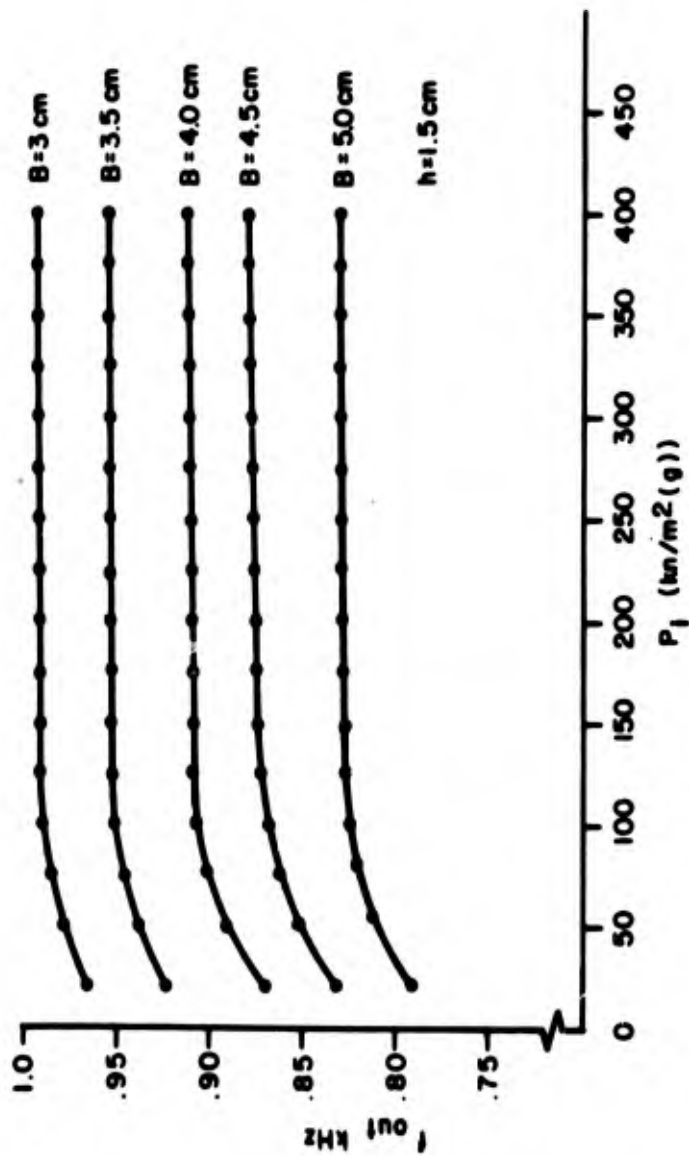
Figure 16. Output frequency versus input pressure.
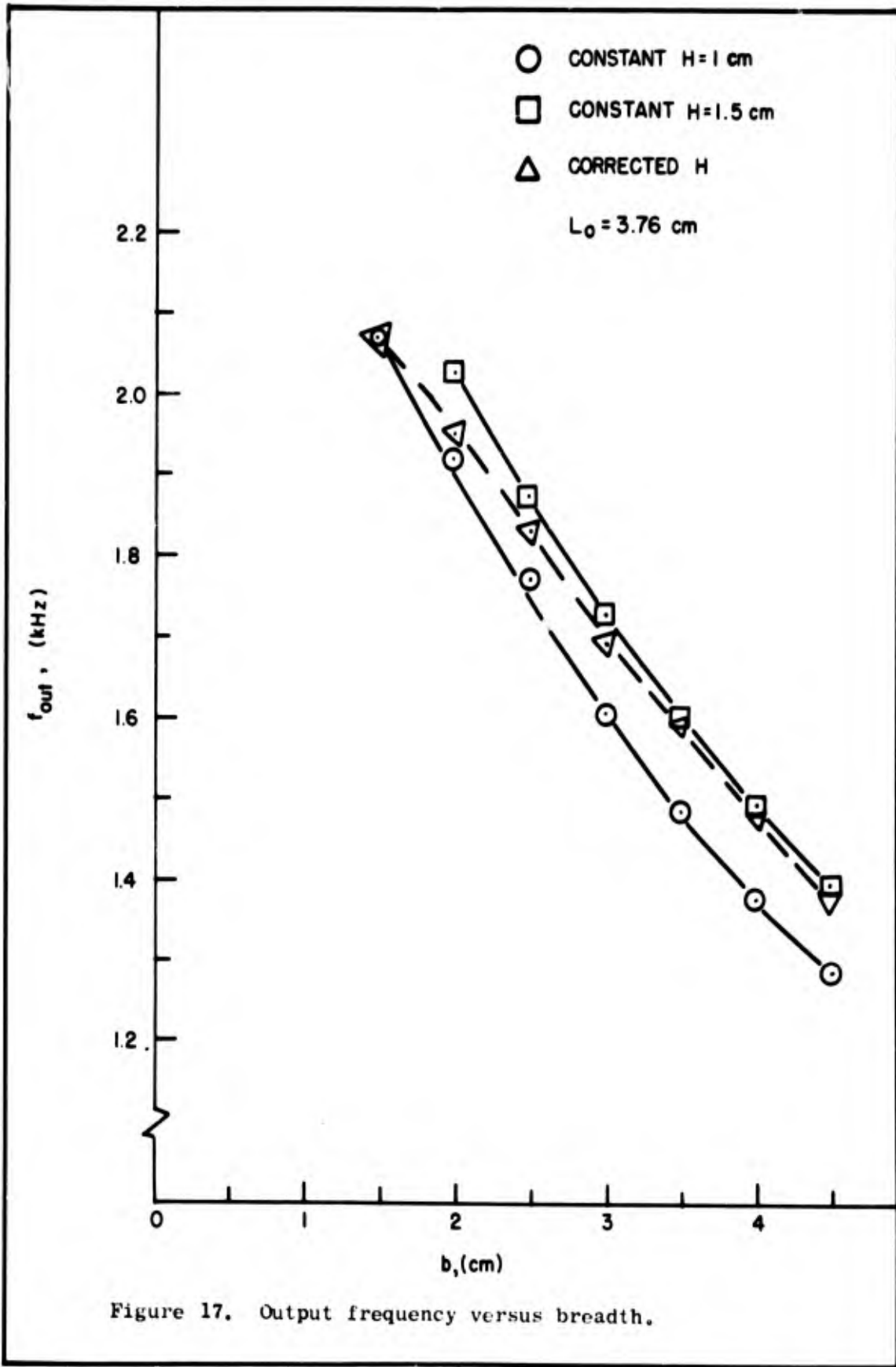
Figure 17. Output frequency versus breadth.

47

Figure 18. Output frequency versus splitter distance for several values of breadth.
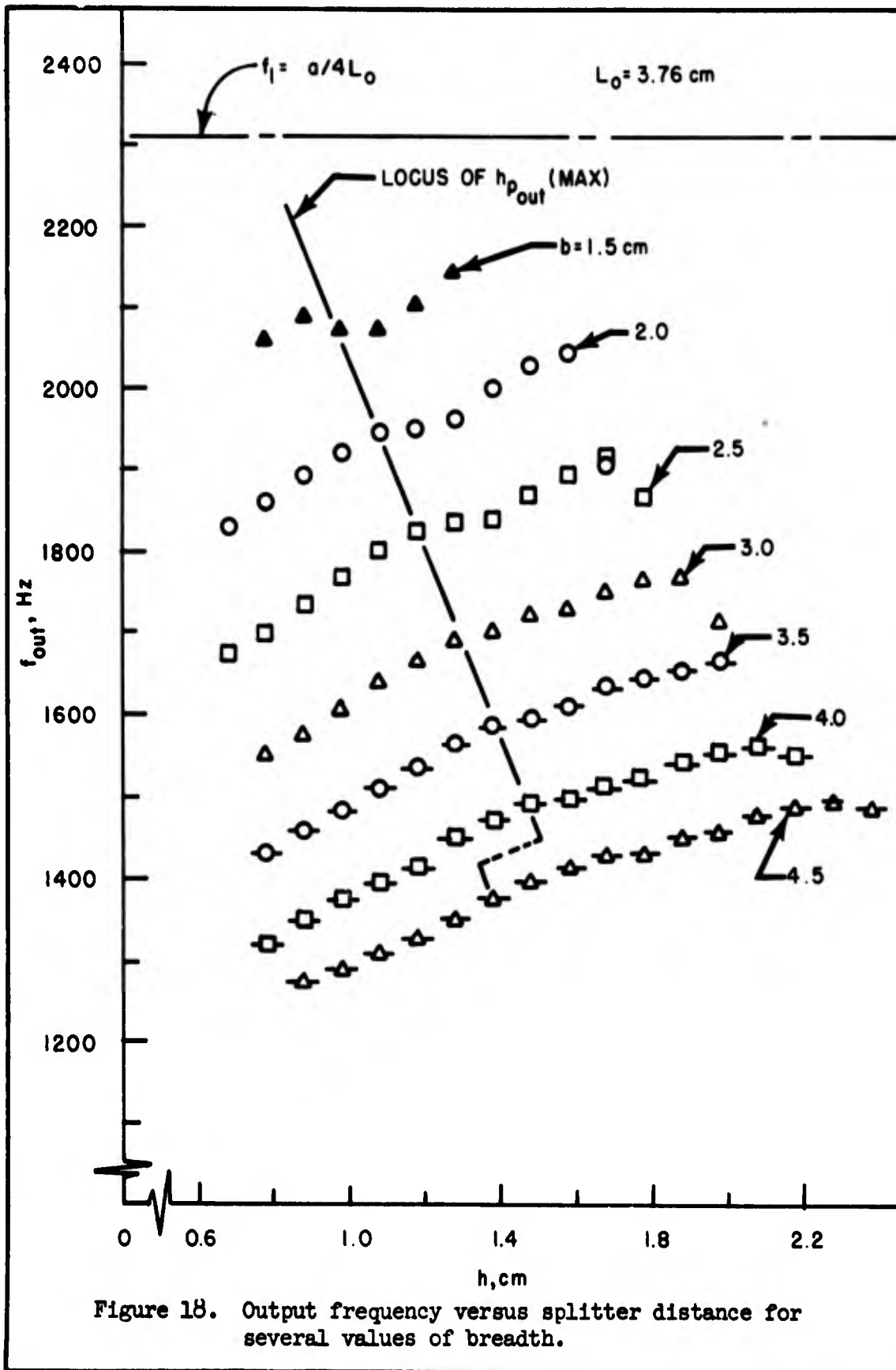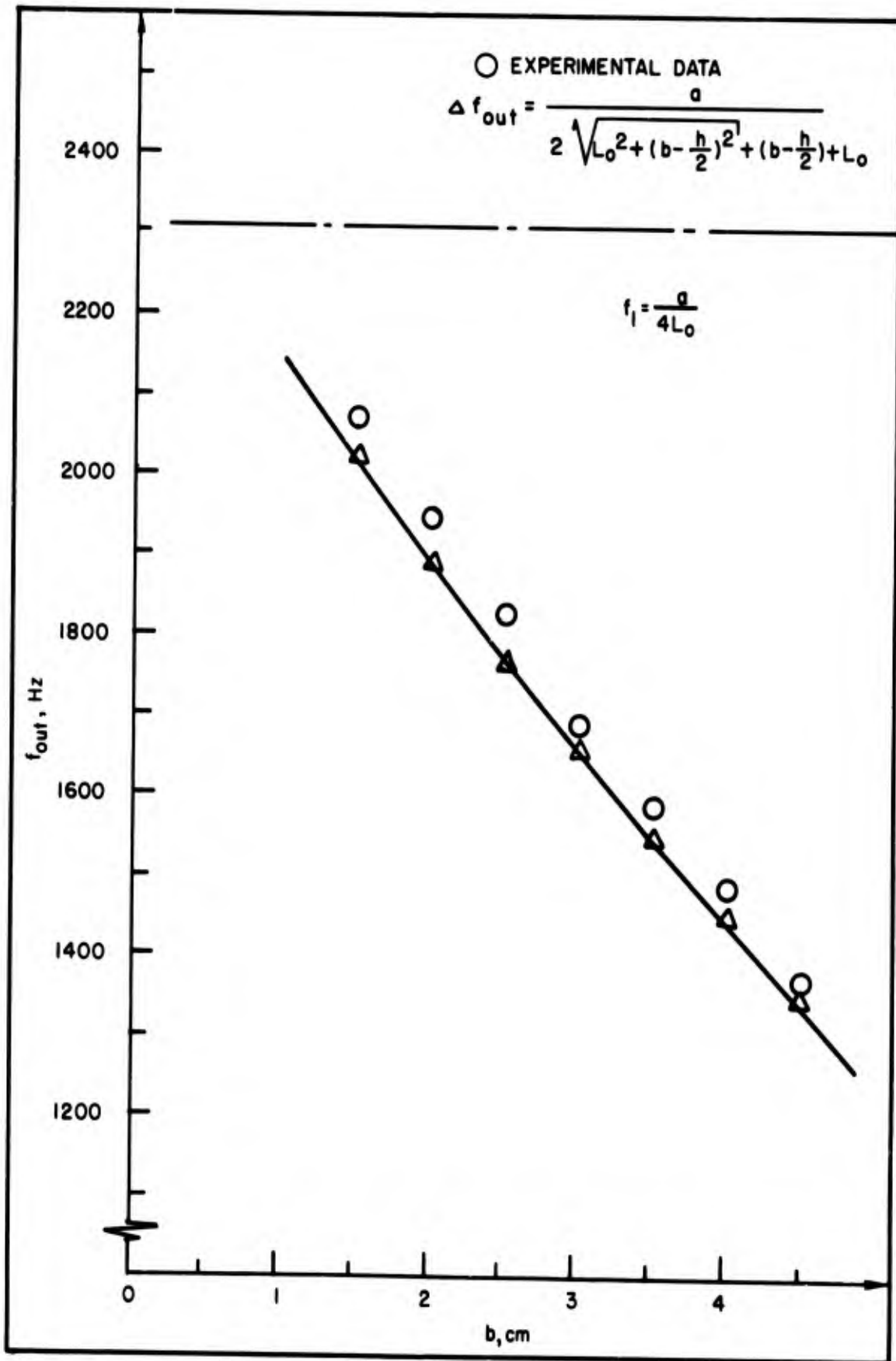
Figure 19. Output frequency versus breadth for maximum amplitude values of h.
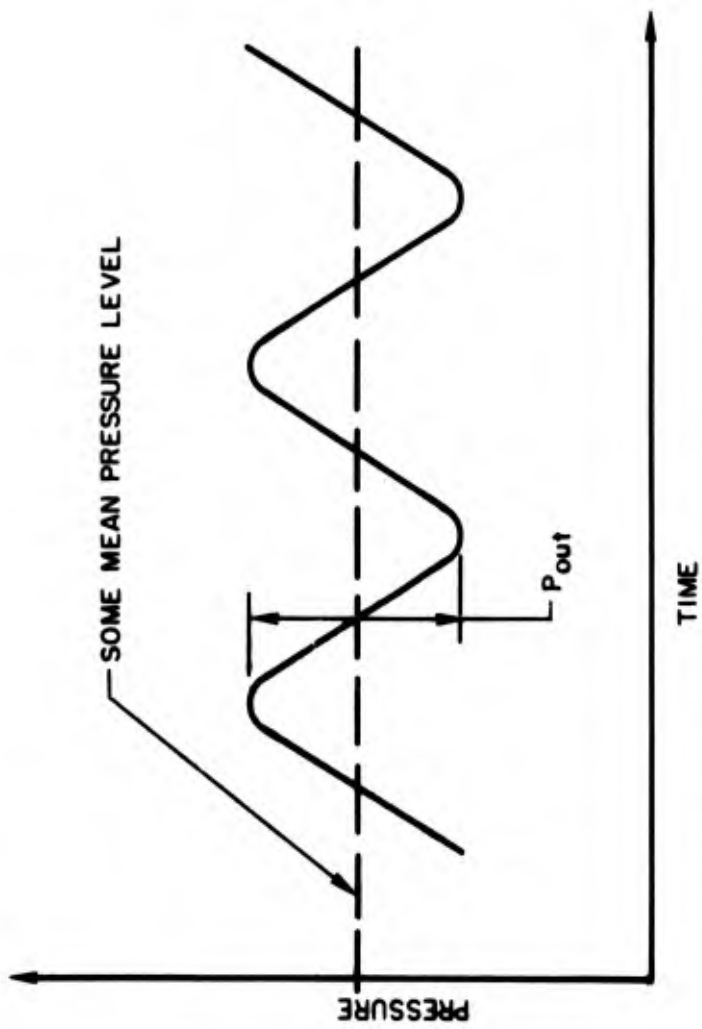
Figure 20. Definition of signal amplitude.
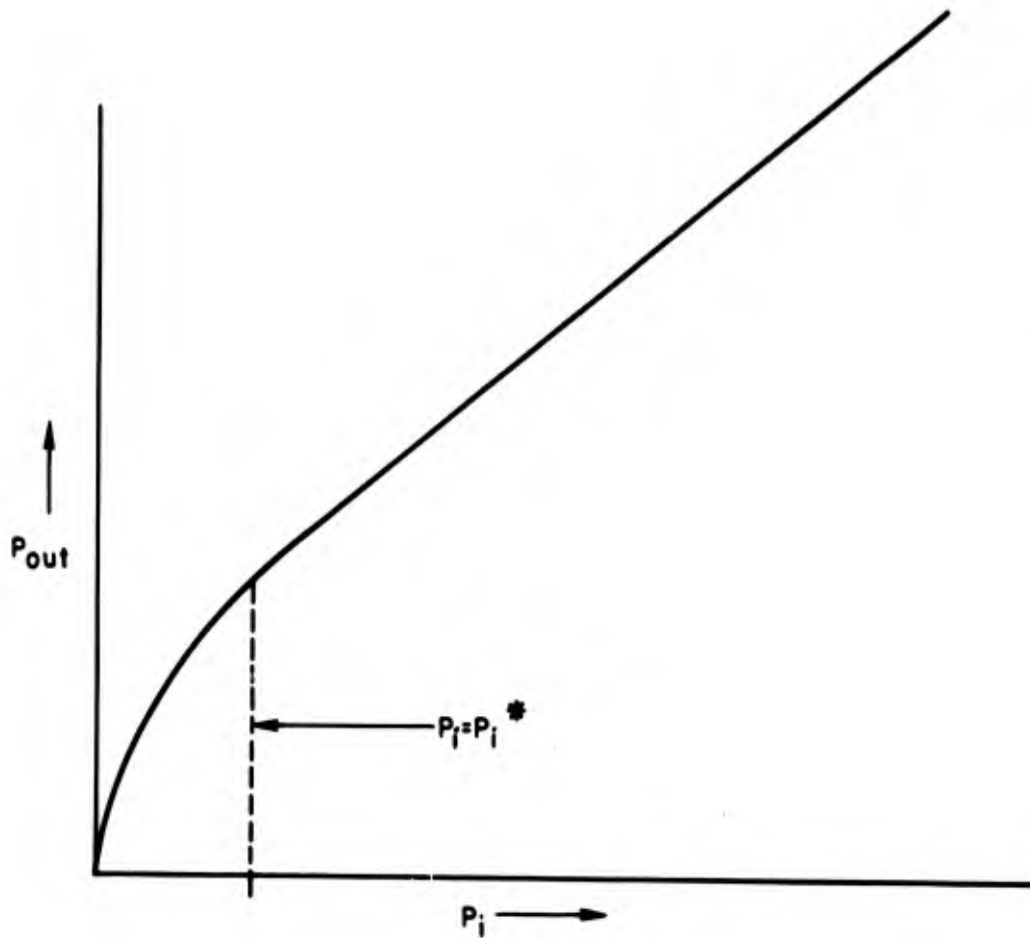
Figure 21. Output signal amplitude versus input pressure.

Figure 22. Signal amplitude versus temperature for three values of input pressure.
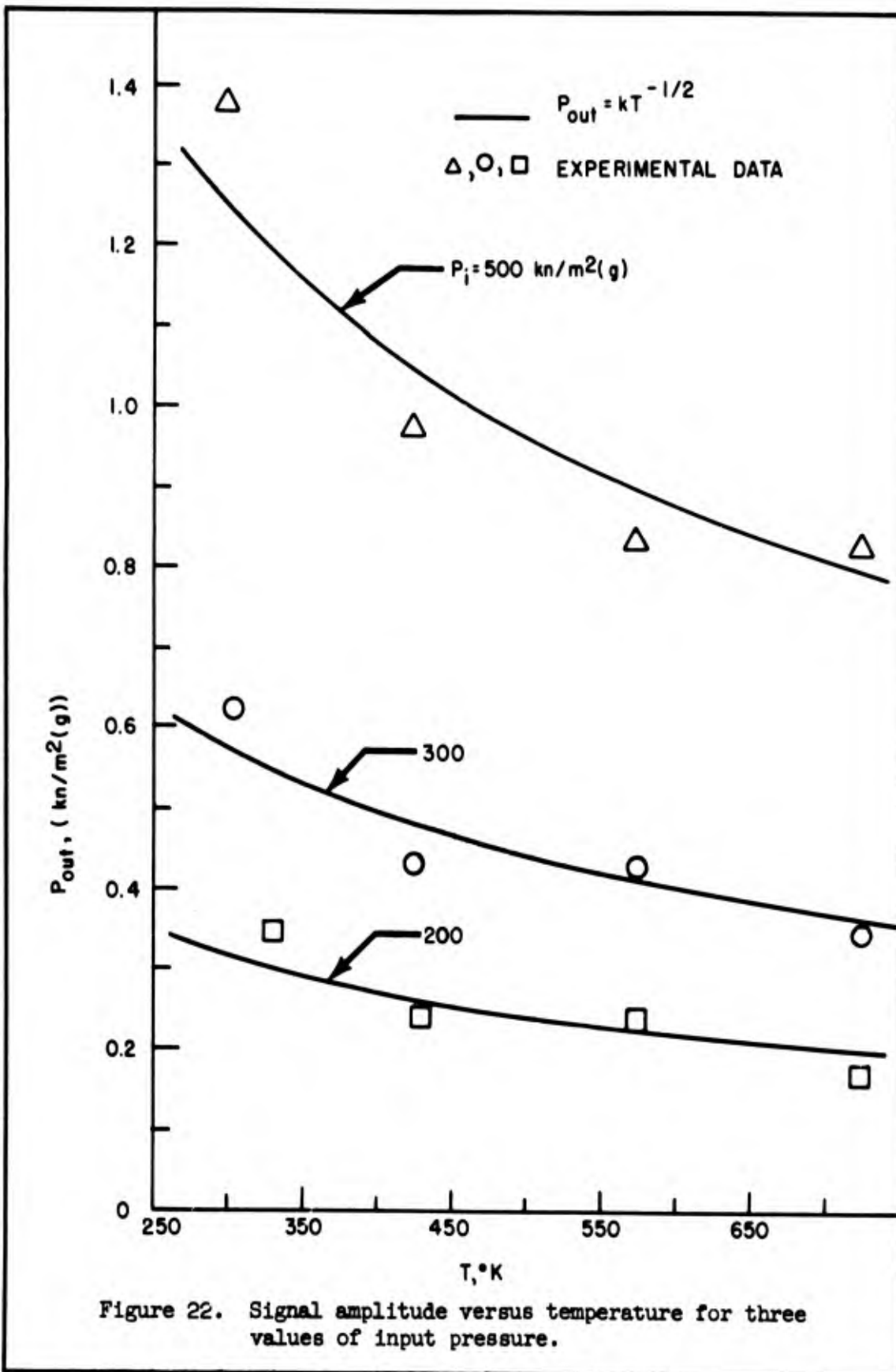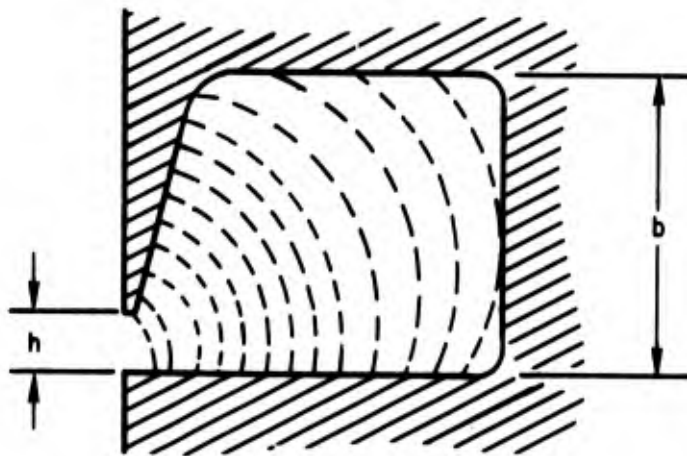
Figure 23. Cylindrical wave behavior for cavity with large
width and small mouth.
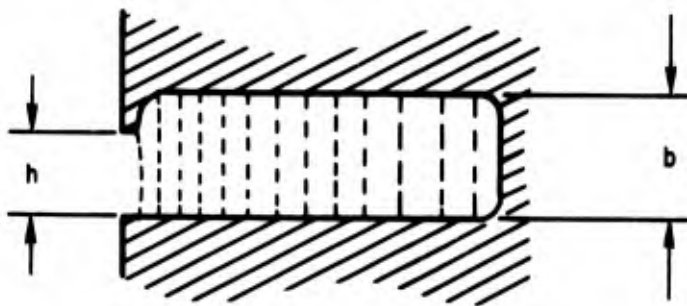
Figure 24. Plane-wave behavior for cavity with small
width and relative large mouth.
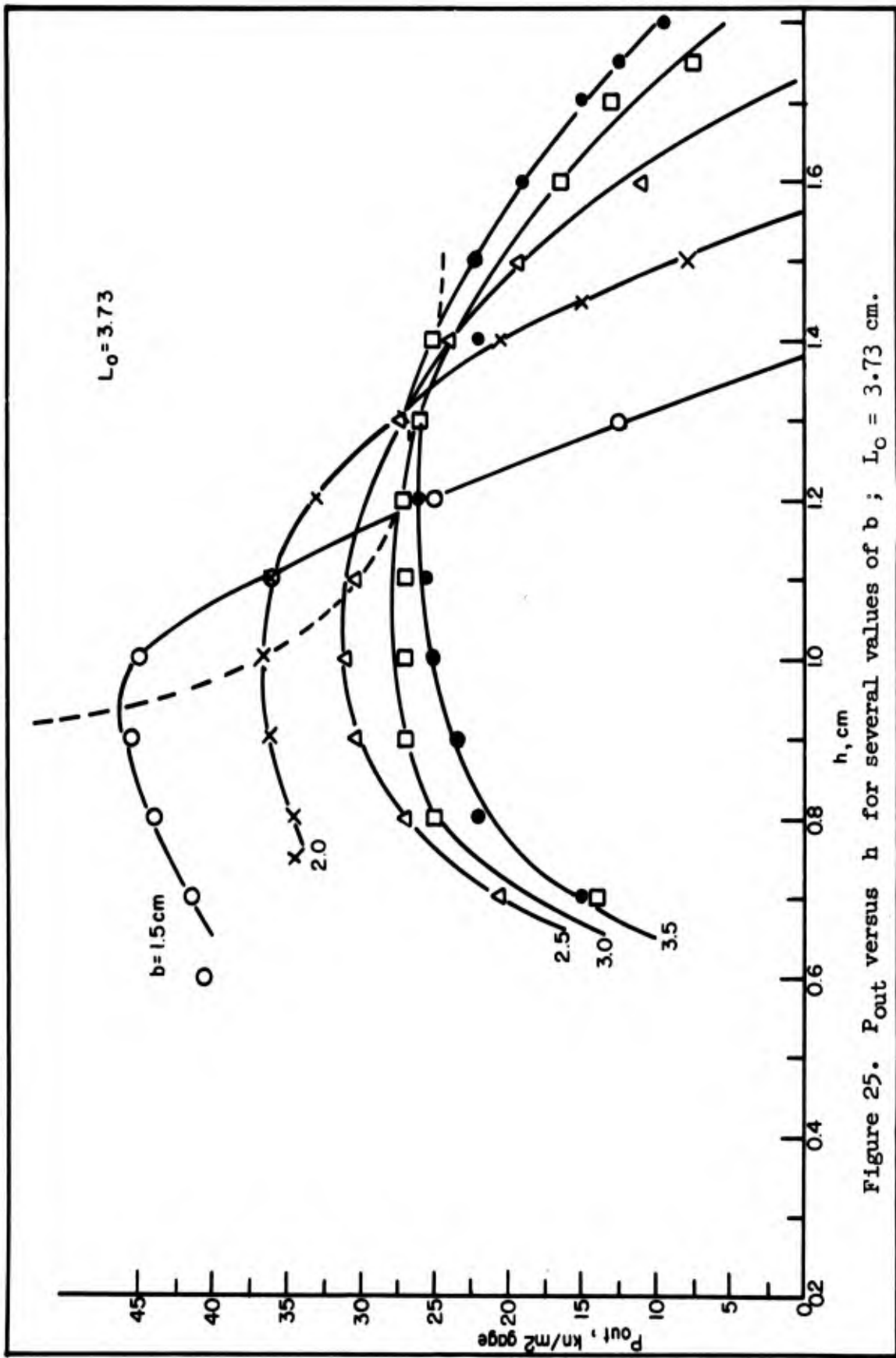
Figure 25. P_{out} versus h for several values of b ; L_o = 3.73 cm.

54
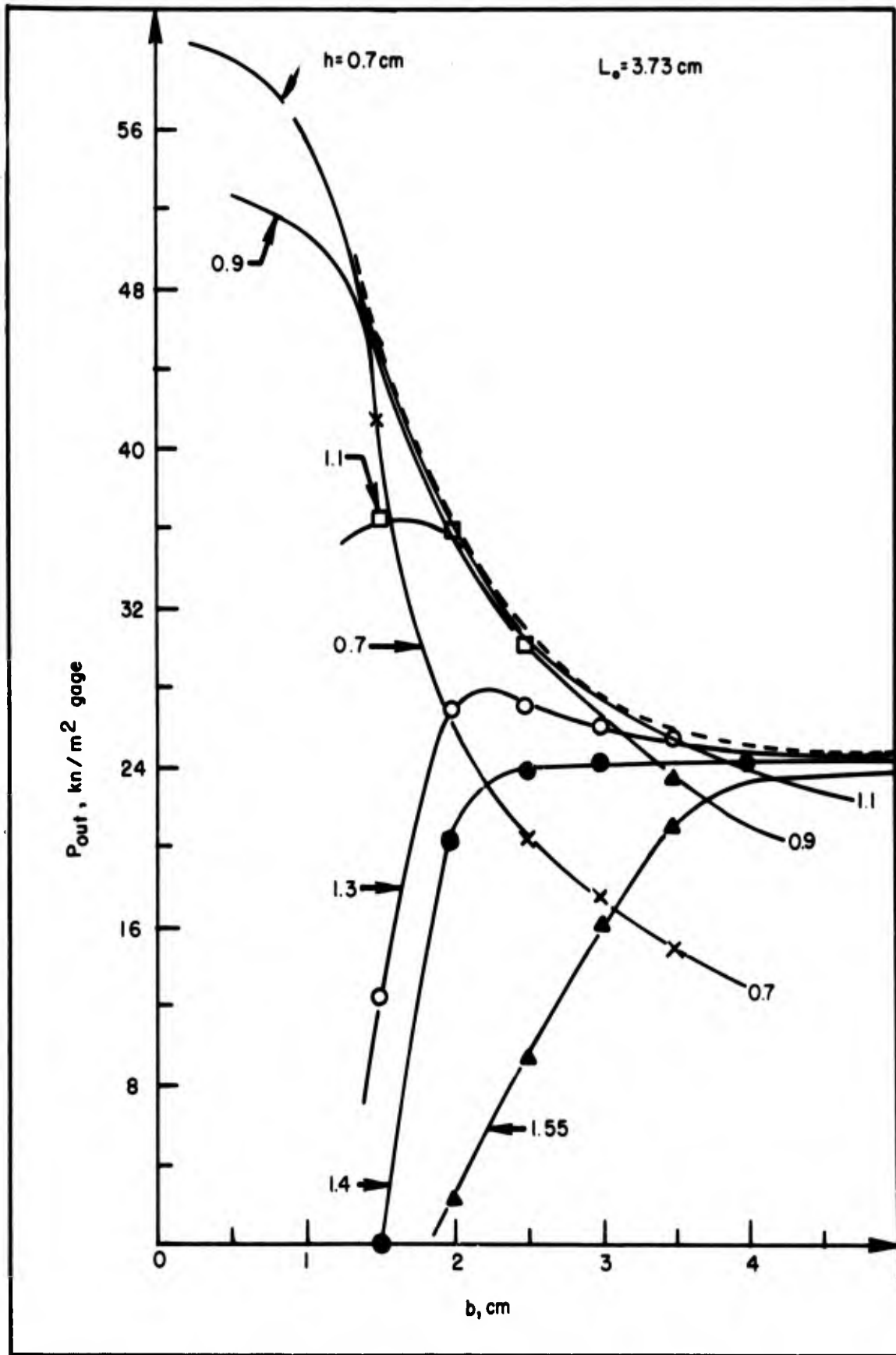
Figure 26 . P_{out} versus b for several values of h: $L_o = 3.73$ cm.
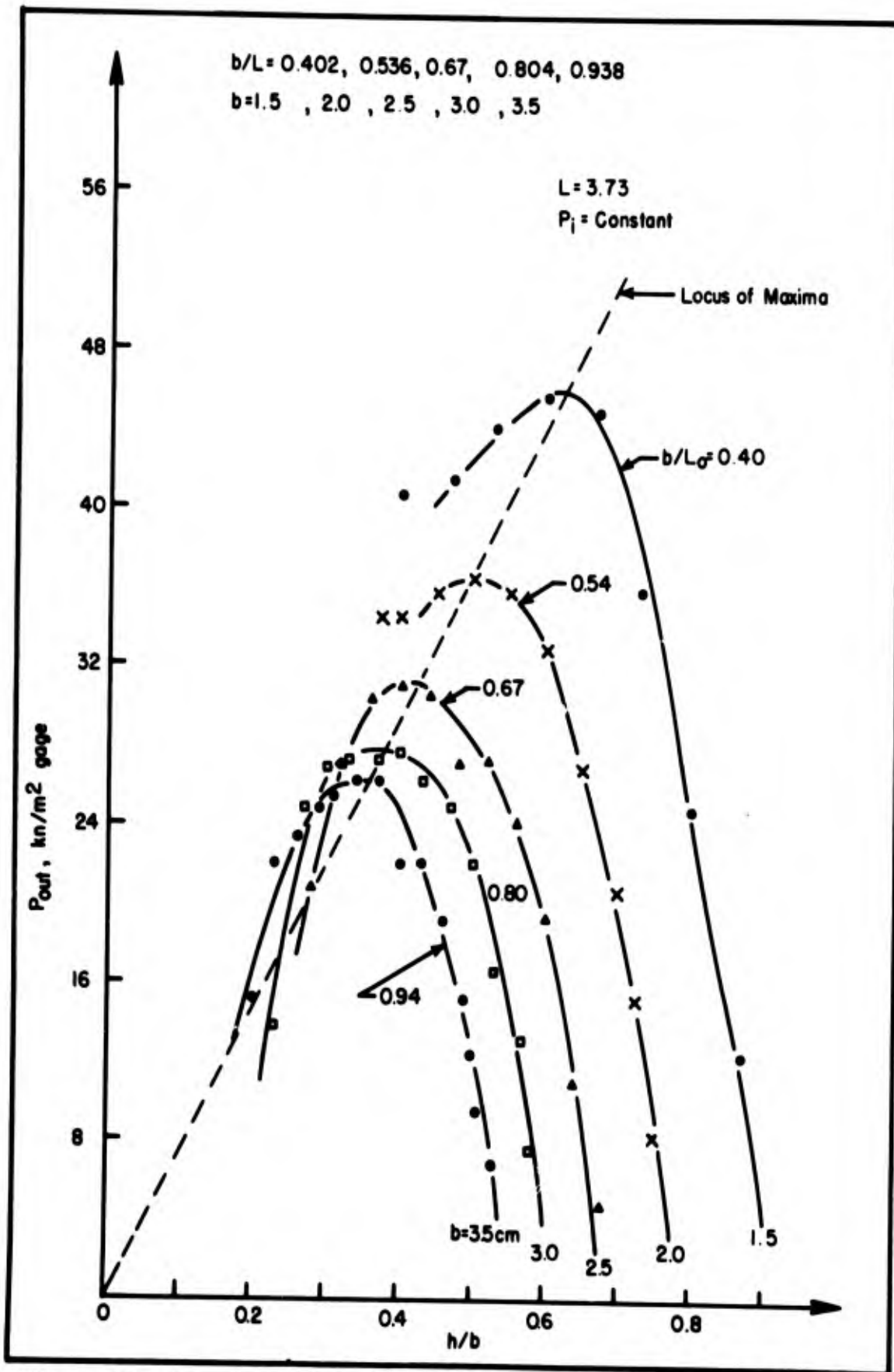
Figure 27. P_{out} versus h/b for several values of b/L_o; L_o = 3.73 cm.
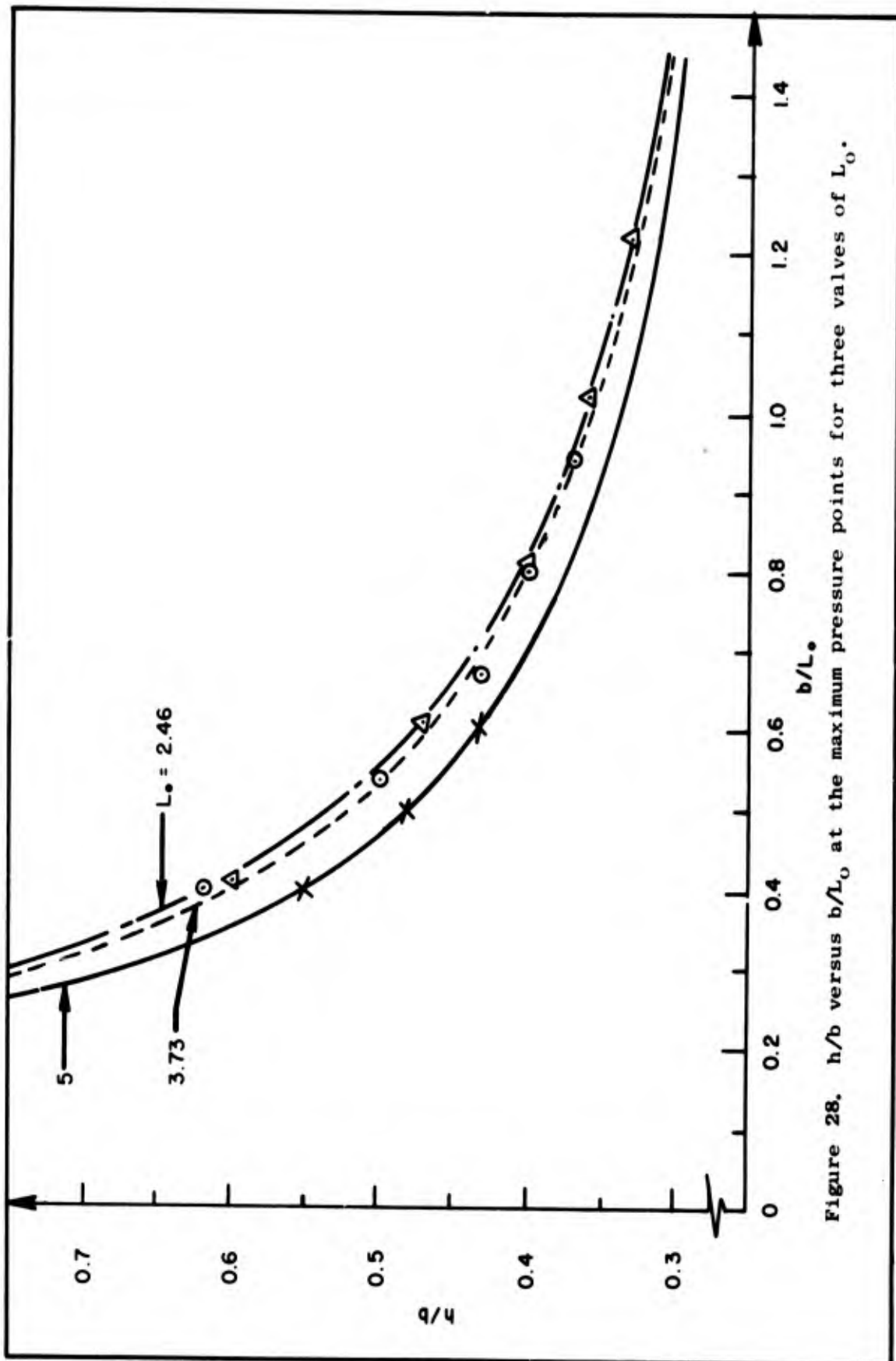
Figure 28. h/b versus b/L_o at the maximum pressure points for three valves of L_o.

57

Figure 29. $P_{out_{Max}}$ versus b/L_0; h/b as a parameter.
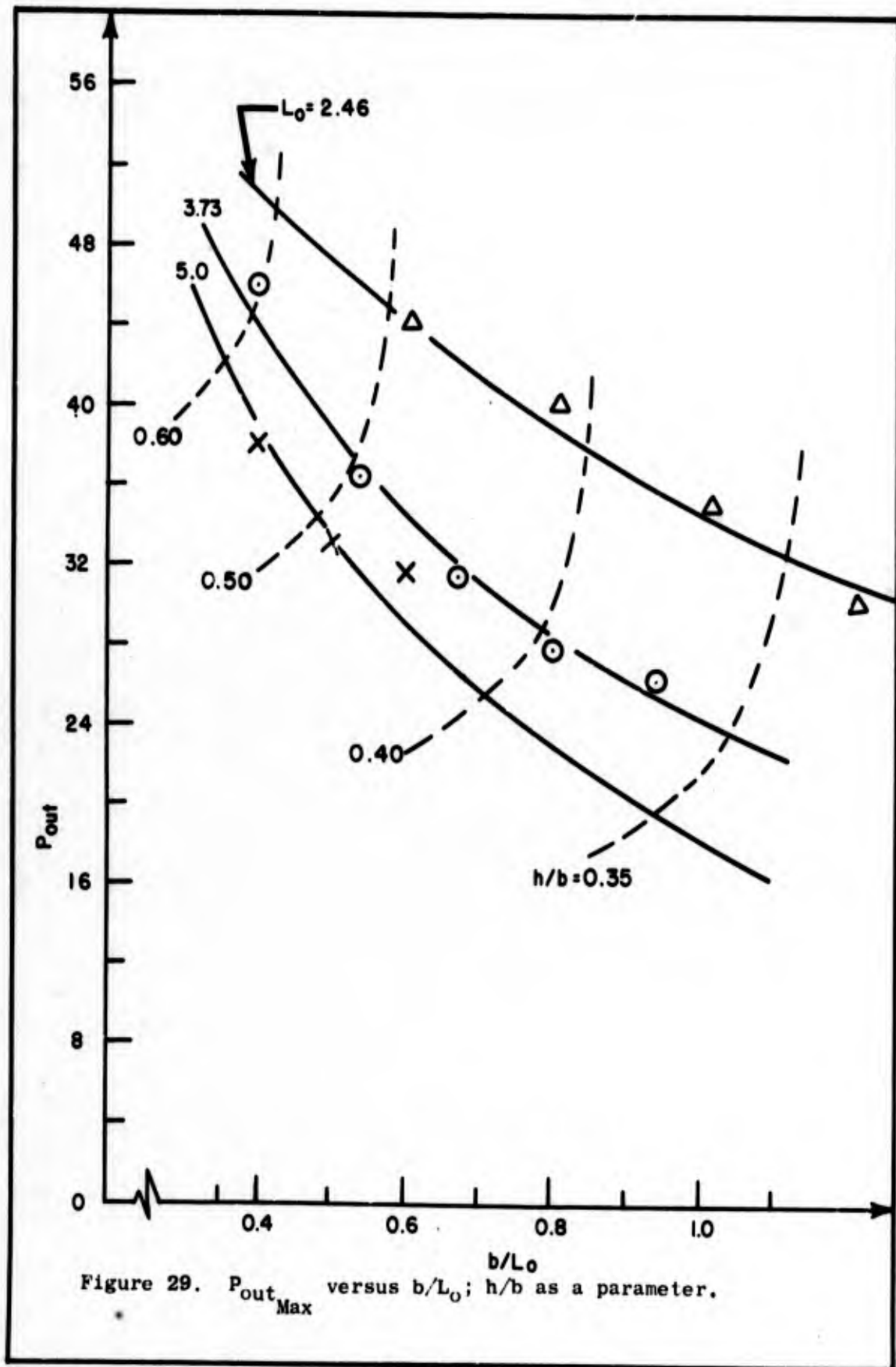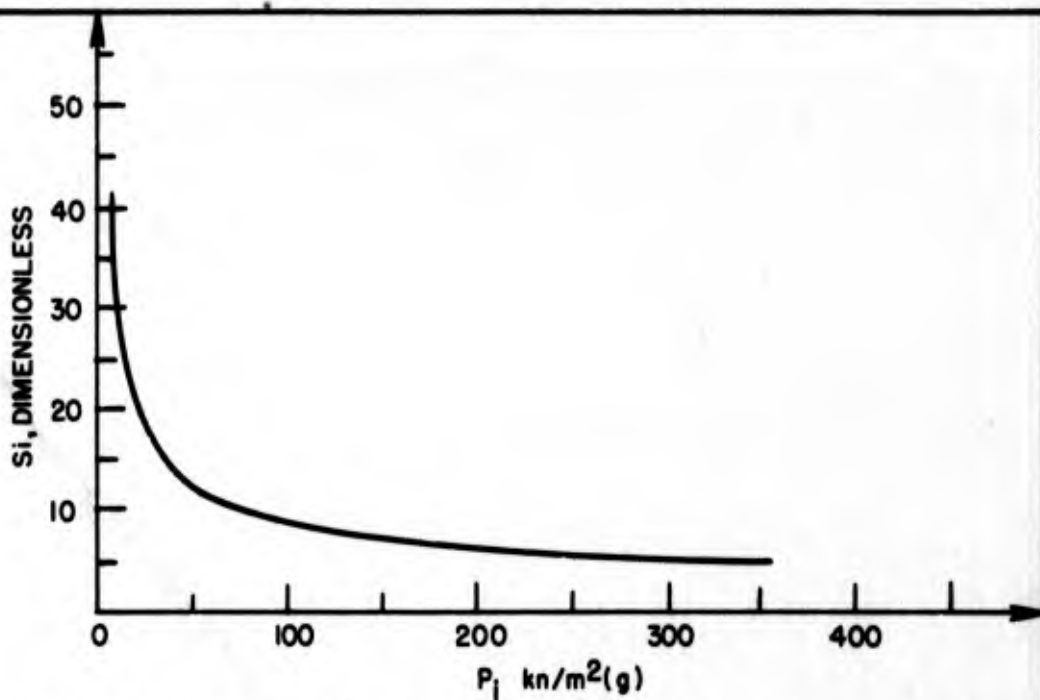
Figure 30. Signal-isolation ratio versus input pressure.
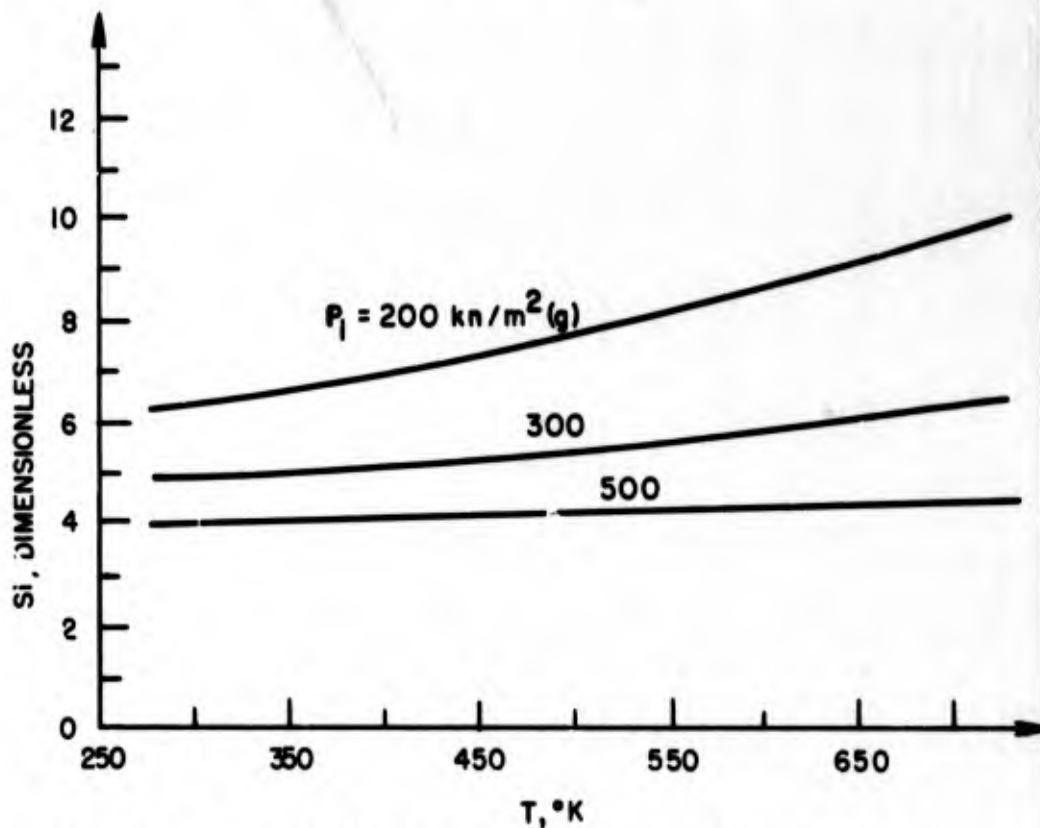
Figure 31. Signal-isolation ratio versus temperature.

59
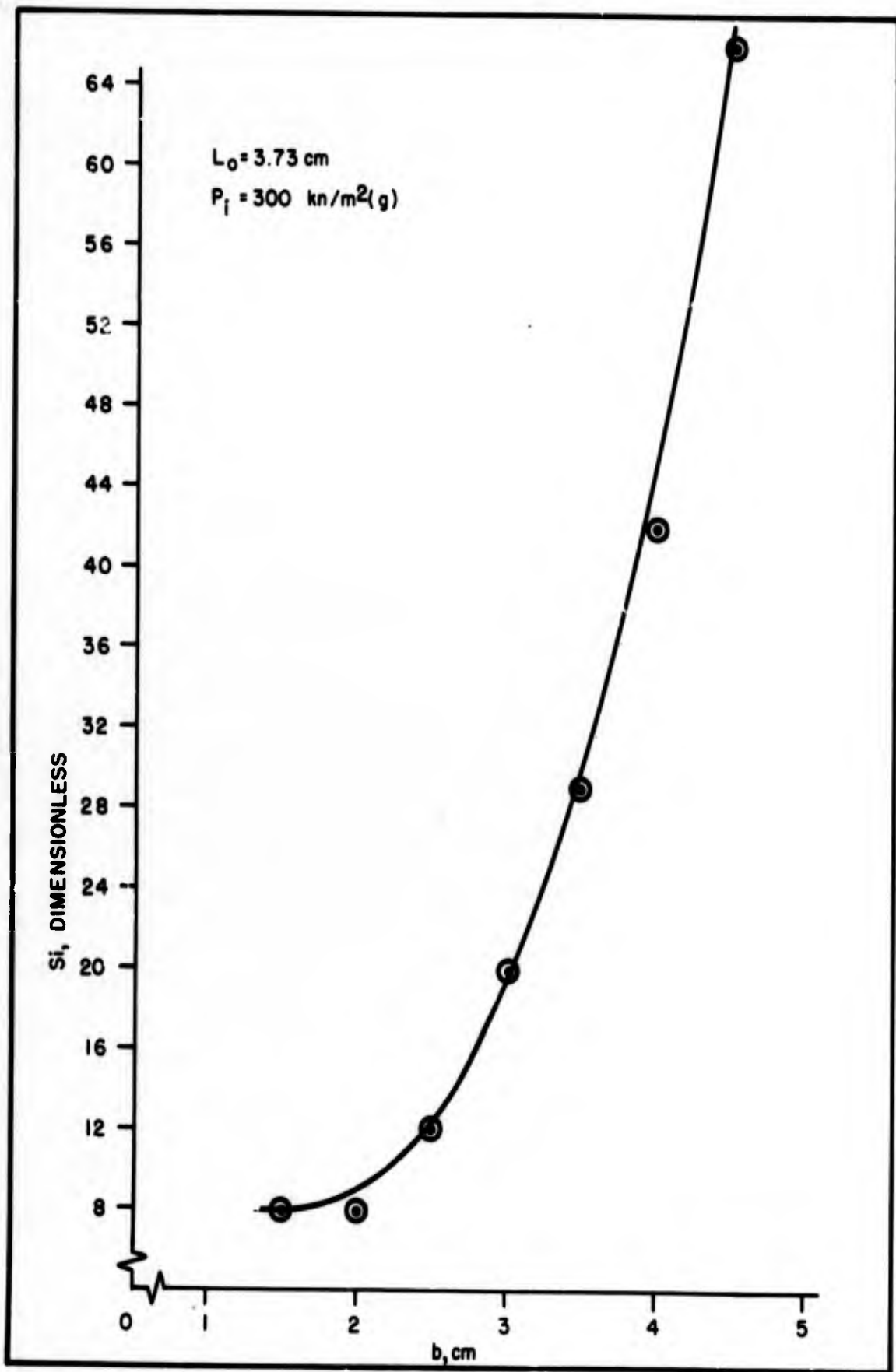
Figure 32. Signal-isolation ratio versus cavity width for maximum amplitude values.
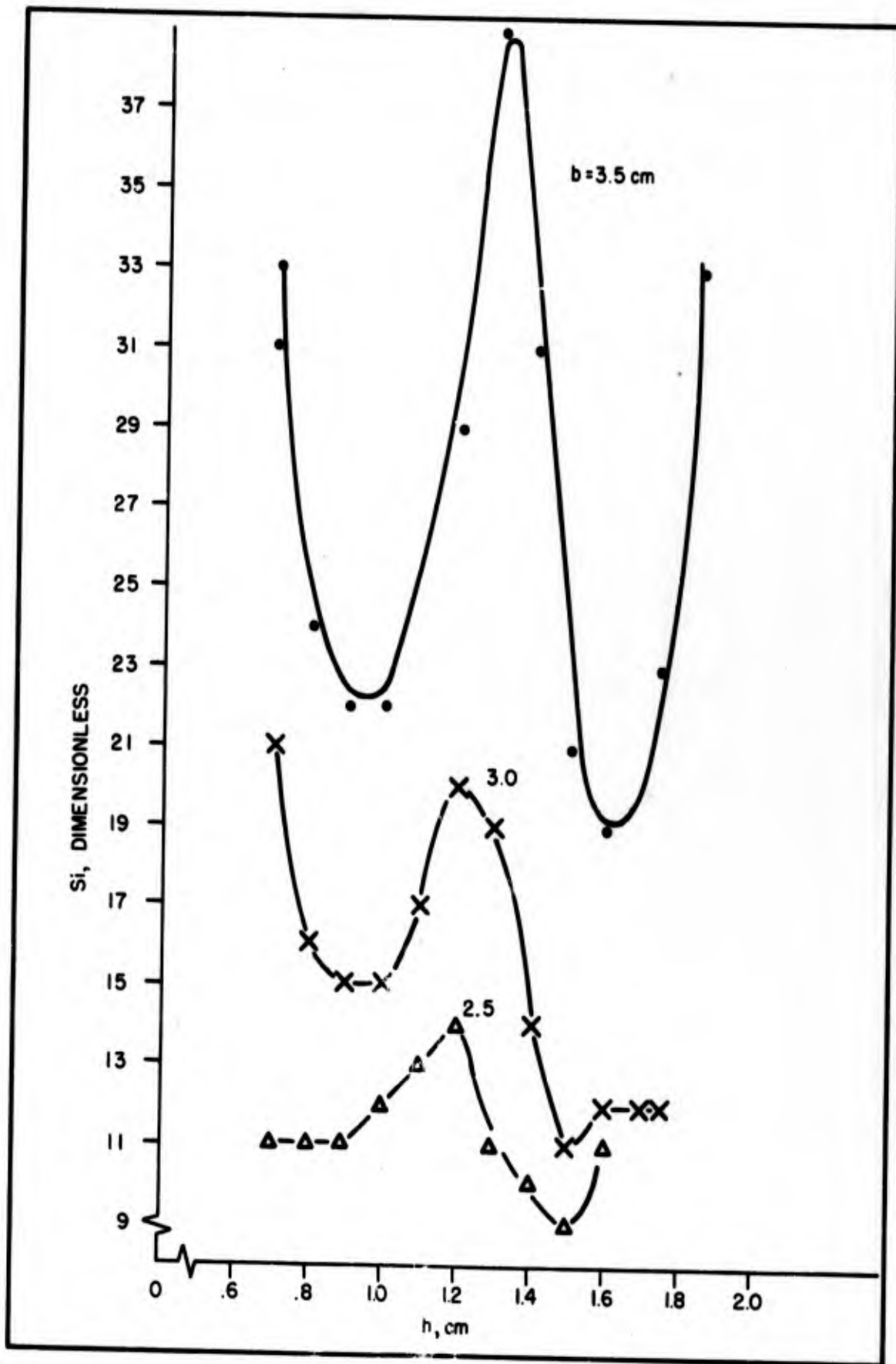
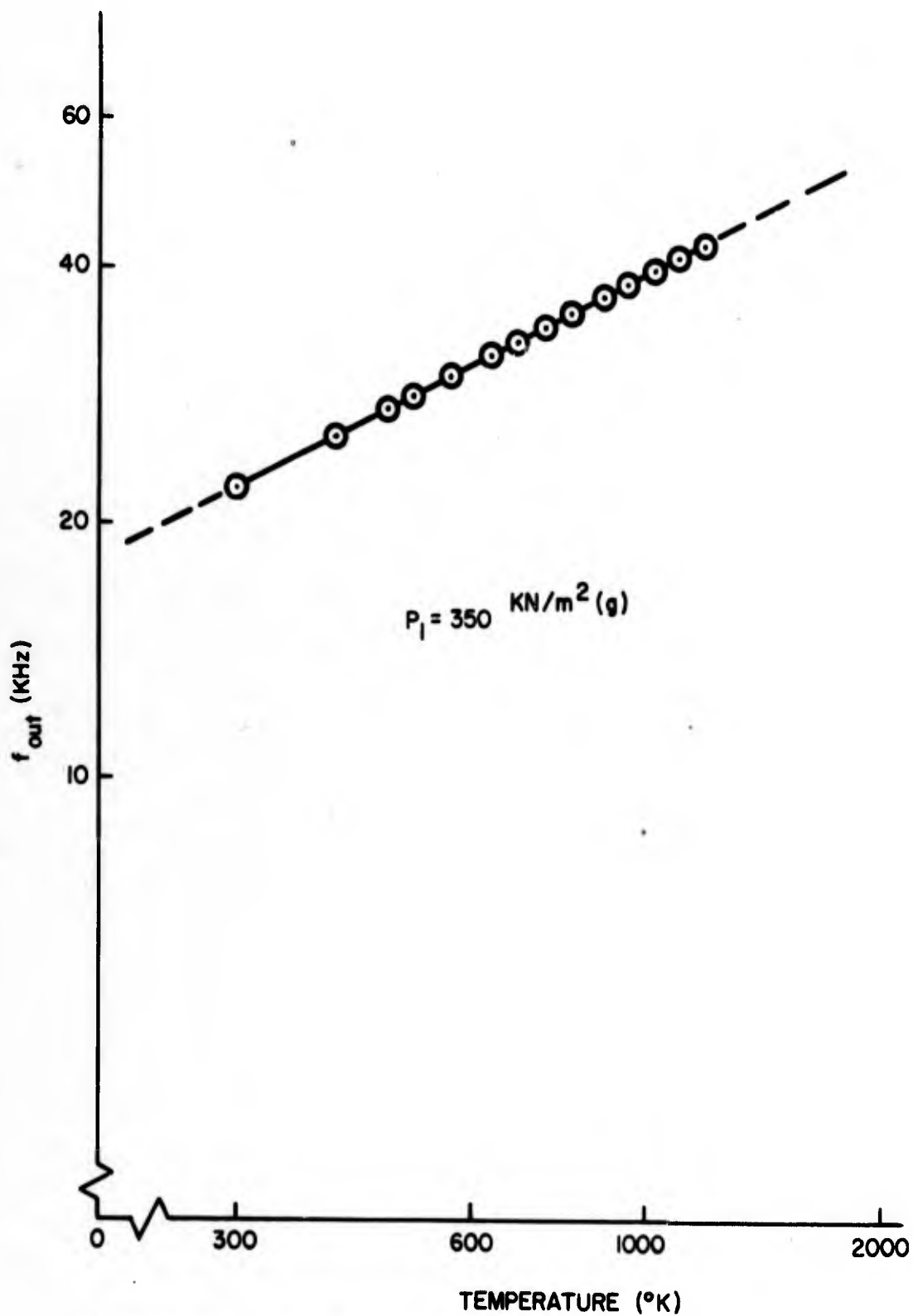Figure 33. Signal-isolation ratio versus splitter distance for three values of cavity width.
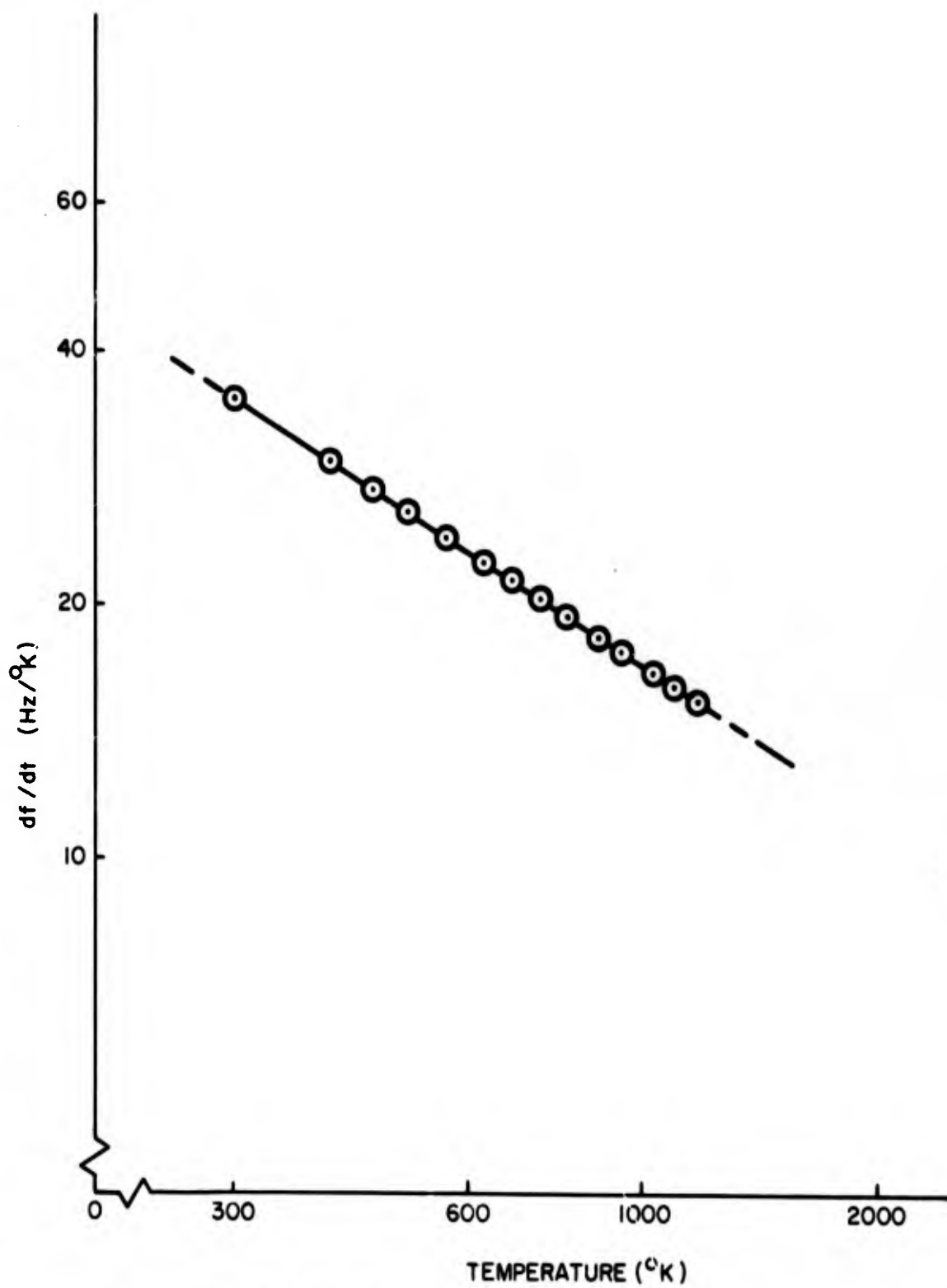
Figure 34. Log-log plot of f_{out} versus T.

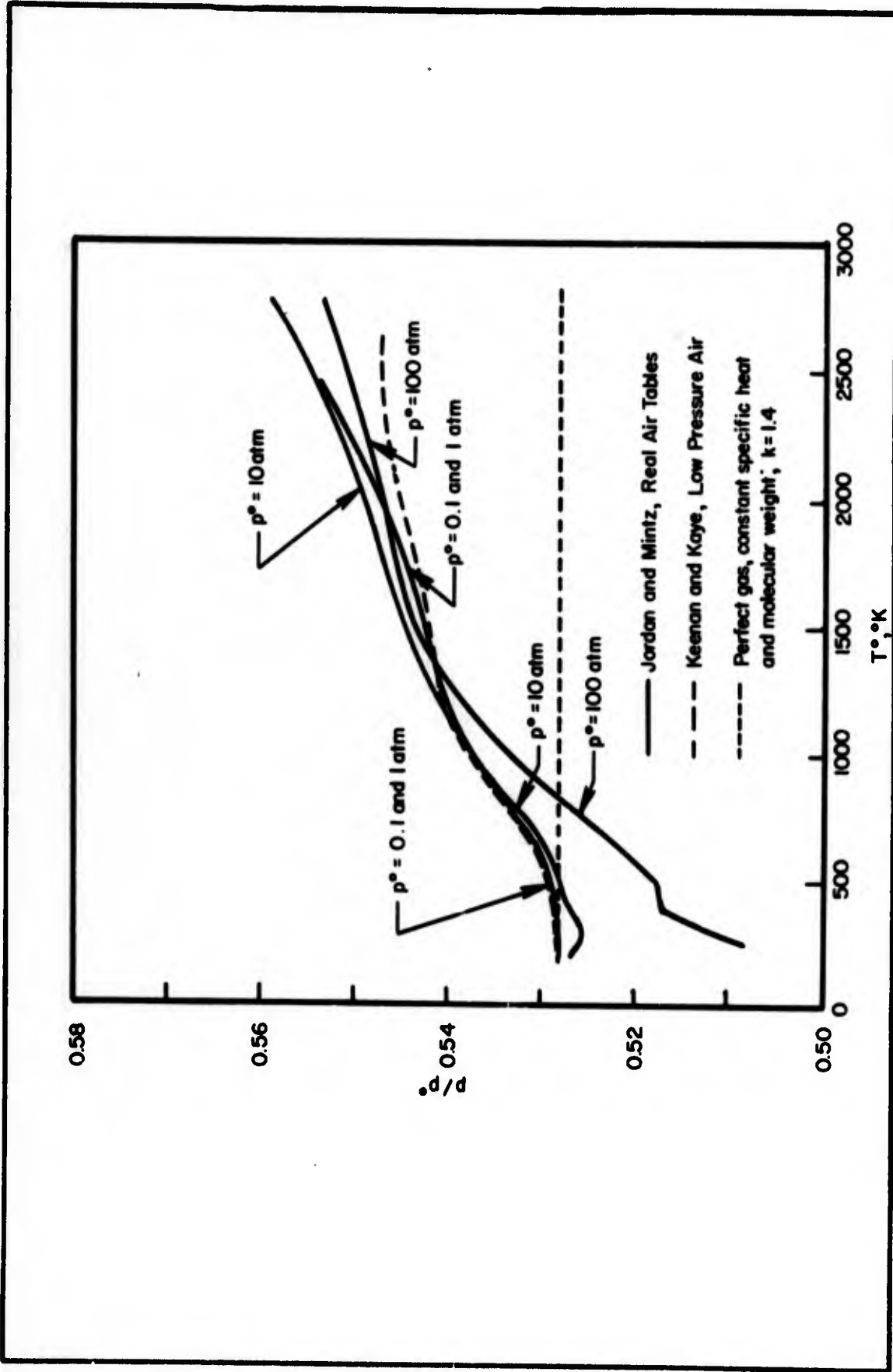Figure 35. Sensitivity df_{out}/dt versus temperature.

63

Figure 36. The ratio of the static pressure to the stagnation pressure as a function of the stagnation temperature and stagnation pressure at Mach 1.
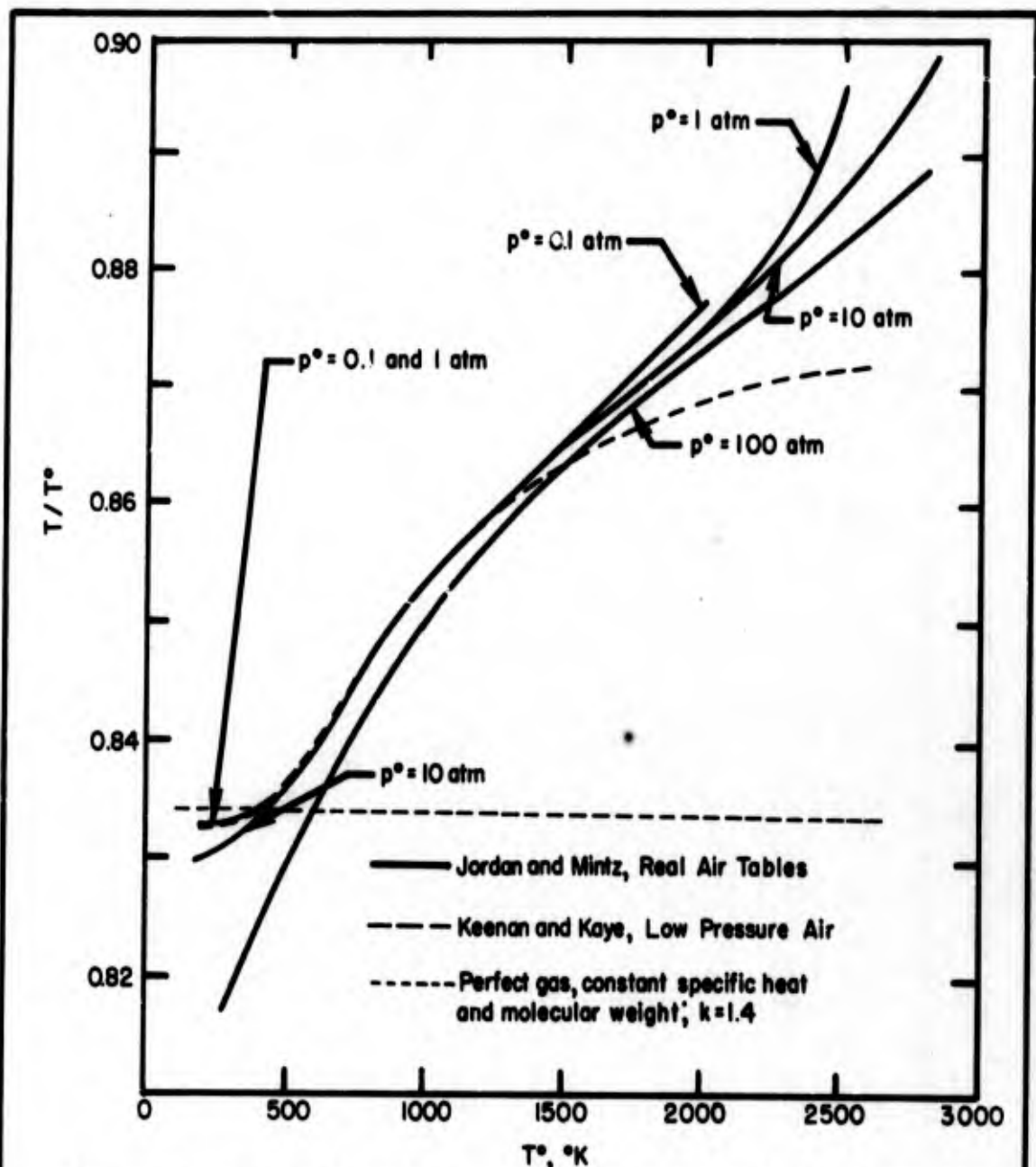
Figure 37. The ratio of the static temperature to the stagnation temperature as a function of the stagnation temperature and the stagnation pressure at Mach 1.
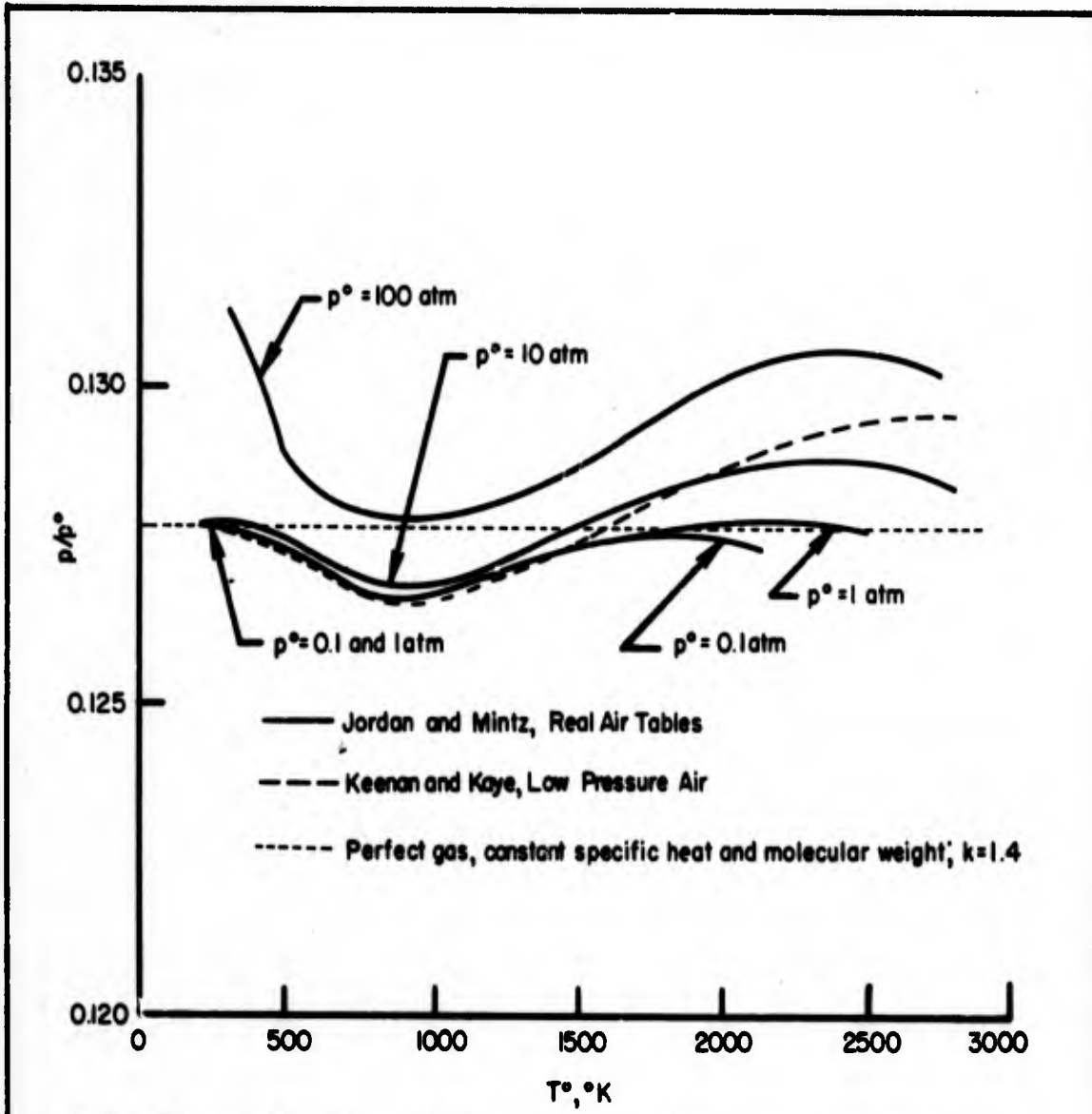
Figure 38. The ratio of the static pressure to the stagnation pressure as a function of the stagnation temperature and the stagnation pressure at Mach 2.
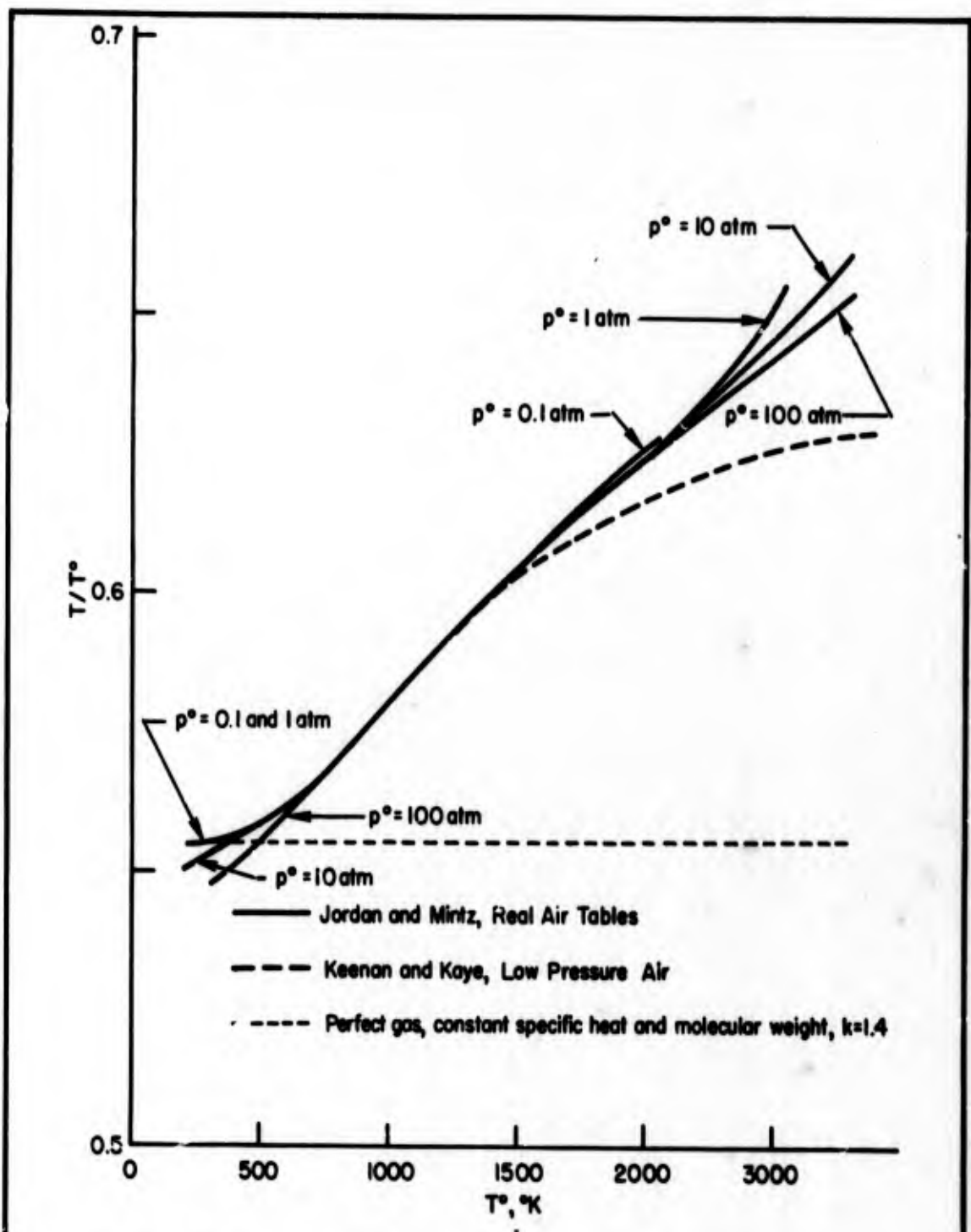
Figure 39. The ratio of the static temperature to the stagnation temperature as a function of the stagnation temperature and the stagnation pressure at Mach 2.
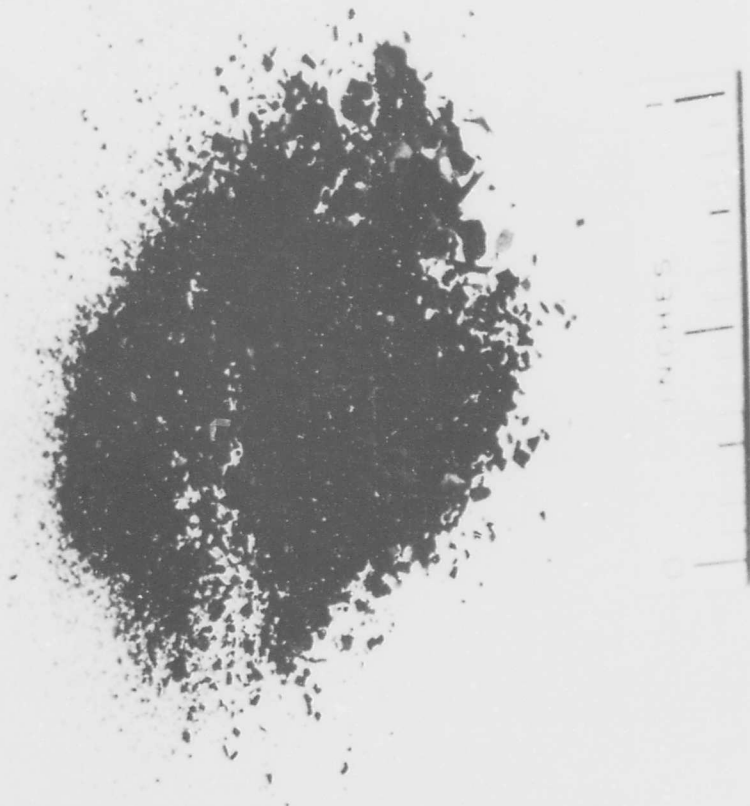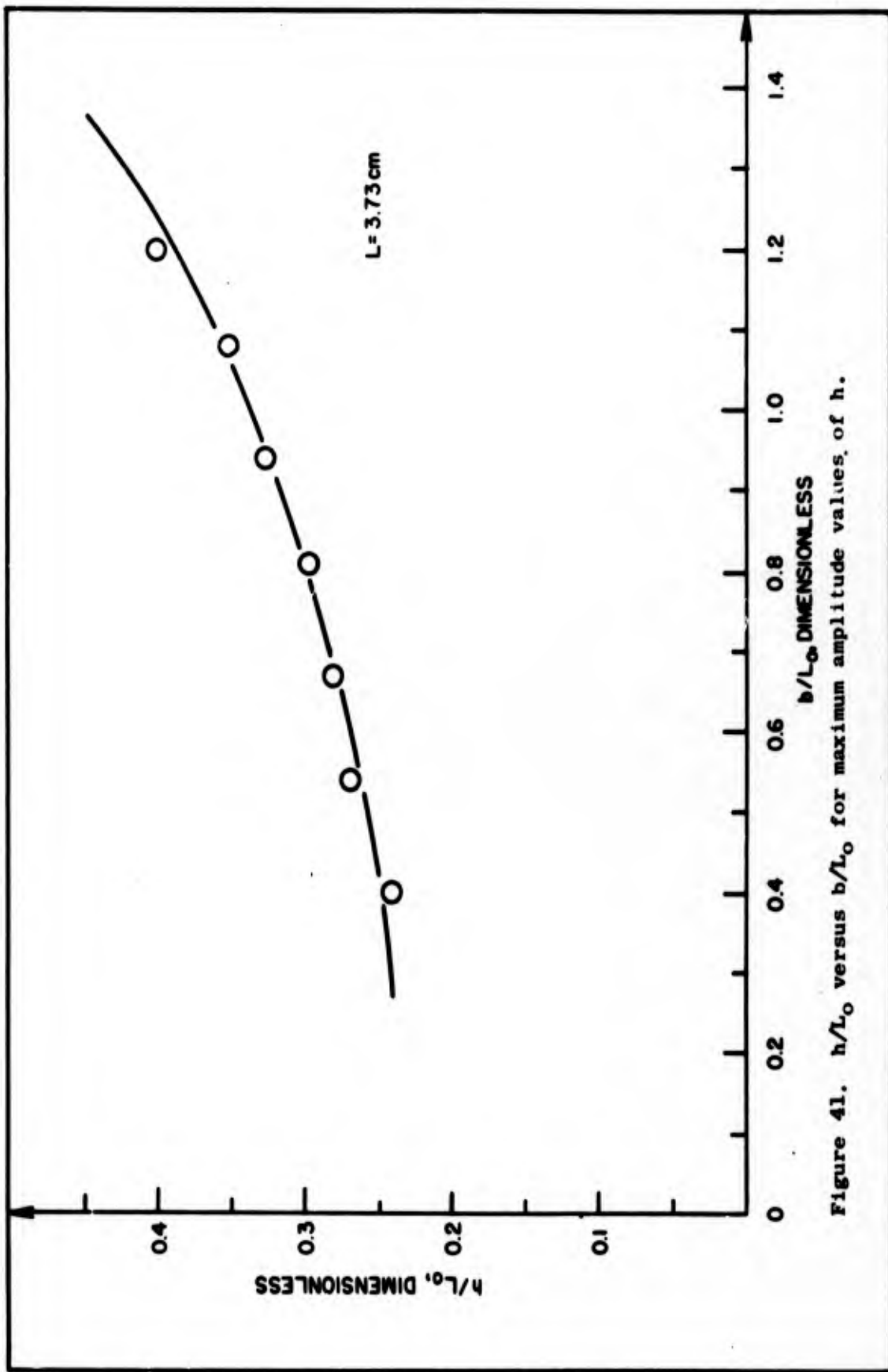
Figure 40. Sample of residue from heating coil.

Figure 41. h/L_o versus b/L_o for maximum amplitude values, of h.

DOCUMENT CONTROL DATA - R & D

(Security classification of title, body of abstract and indexing annotation must be entered when the overall report is classified)

1. ORIGINATING ACTIVITY *(Corporate author)*	2a. REPORT SECURITY CLASSIFICATION
Harry Diamond Laboratories Washington, D. C., 20438	UNCLASSIFIED
	2b. GROUP

3. REPORT TITLE

Fluerics
27. Flueric Temperature-Sensing Oscillator Design

4. DESCRIPTIVE NOTES *(Type of report and inclusive dates)*

5. AUTHOR(S) *(First name, middle initial, last name)*

Wilmer Gaylord and Vondell Carter

6. REPORT DATE	7a. TOTAL NO. OF PAGES	7b. NO. OF REFS
April 1969	84	7
8a. CONTRACT OR GRANT NO.	**9a. ORIGINATOR'S REPORT NUMBER(S)**	
b. PROJECT NO. DA-1P014501A33B	TR-1428	
c. AMCMS Code: 5011.11.71200	9b. OTHER REPORT NO(S) *(Any other numbers that may be assigned this report)*	
d. HDL Proj: 31100		

10. DISTRIBUTION STATEMENT

This document has been approved for public release and sale; its distribution
is unlimited.

11. SUPPLEMENTARY NOTES	12. SPONSORING MILITARY ACTIVITY
	U. S. Army Aviation Laboratories Fort Eustis, Virginia and

13. ABSTRACT

Air Force Propulsion Laboratory
Aeronautical Systems Division
Wright-Patterson Air Force Base, Ohio

Studies have been conducted at the Harry Diamond Laboratories to determine the
dependence of output-signal characteristics on cavity (resonator) dimensions of
flueric temperature-sensing oscillators. The effects of resonator dimensions
(length and width), of nozzle area ratio, and of edge distance from the inlet nozzle
on the operational threshold, frequency, amplitude, and signal-isolation ratio were
studied.

The information derived can be utilized to make the process of flueric
temperature sensor-oscillator design a more precise and scientific operation.
Experimental data have been arranged to show the relationship of signal character-
istics to resonator configuration (dimensions) and environment (pressure and
temperature).

DD FORM 1473 REPLACES DD FORM 1473, 1 JAN 64, WHICH IS
OBSOLETE FOR ARMY USE.

14. KEY WORDS	LINK A		LINK B		LINK C	
	ROLE	WT	ROLE	WT	ROLE	WT
Temperature sensor	8	3				
Flueric oscillator	10	3				